Hypoxia-induced tracheal elasticity in vector beetle facilitates the loading of pinewood nematode

Xuan Tang[1,2], Jiao Zhou[1], Tuuli-Marjaana Koski[1], Shiyao Liu[1,2], Lilin Zhao[1,2]*, Jianghua Sun[3,1]*

[1]State Key Laboratory of Integrated Management of Pest Insects and Rodents, Institute of Zoology, Chinese Academy of Sciences, Beijing 1000101, China.

[2]University of Chinese Academy of Sciences, Beijing 100049, China.

[3]College of Life Science, Institute of Life Science and Green Development, Hebei University, Baoding 071002, China.

These authors contributed equally: Xuan Tang, Jiao Zhou, Tuuli-Marjaana Koski.

*Corresponding author. Email: sunjh@hbu.edu.cn (J.S.); zhaoll@ioz.ac.cn (L.Z.)

Abstract

Many pathogens rely on their insect vectors for transmission. Such pathogens are under selection to improve vector competence for their transmission by employing various tissue or cellular responses of vectors. However, whether pathogens can actively cause hypoxia in vectors and exploit hypoxia responses to promote their vector competence is still unknown. Fast dispersal of pinewood nematode (PWN), the causal agent for the destructive pine wilt disease and subsequent infection of pine trees is characterized by the high vector competence of pine sawyer beetles (*Monochamus spp.*), and a single beetle can harbor over 200,000 PWNs in its tracheal system. Here, we demonstrate that

PWN loading activates hypoxia in tracheal system of the vector beetles. Both PWN loading and hypoxia enhanced tracheal elasticity and thickened the apical extracellular matrix (aECM) of the tracheal tubes while a notable upregulated expression of a resilin-like mucin protein Muc91C was observed at the aECM layer of PWN-loaded and hypoxic tracheal tubes. RNAi knockdown of *Muc91C* reduced tracheal elasticity and aECM thickness under hypoxia conditions and thus decreasing PWN loading. Our study suggests a crucial role of hypoxia-induced developmental responses in shaping vector tolerance to the pathogen and provides clues for potential molecular targets to control pathogen dissemination.

Introduction

Insect vectors are obligatory for the dispersal of many pathogens, including several viruses and parasites deleterious to plant and animal health. Vector competence is pivotal for the successful pathogen arrival and infection of the target host, and is determined by a sophisticated set of direct interactions as pathogens enter, spread, replicate and retain within vector cells and tissues (Bartholomay and Michel, 2018; Gray et al., 2019; Lataillade et al., 2020). Therefore, pathogens have evolved to modulate various defensive responses of vectors, such as autophagy or apoptosis, as has been shown in some leafhoppers, whitefly and mosquitoes, to influence vector competence (Chen et al., 2017; O'neill et al., 2015; Wang et al., 2020). Although understanding the responses that pathogens induce to manipulate vector competence is

important for developing efficient management strategies, the underlying mechanism remains largely elusive.

A pathogen of pine trees, *Bursaphelenchus xylophilus*, commonly known as pine wood nematode (PWN), is transmitted by cerambycid beetles of the genus *Monochamus* and causes pine wilt disease in millions of hectares of pine forests across Asia and Europe (Akbulut and Stamps, 2012). PWN's life cycle has two distinct developmental phases, namely the propagative stage (L_1-L_4 juveniles and reproductive adult) that propagates inside pine trees and the dispersal stage (L_{III} and L_{IV} juveniles) characterized by its close relationship with the vector beetle that transports the nematode to new host trees (Aikawa, 2008; Zhao et al., 2014). The dispersal L_{IV} enters the tracheal system of the adult beetle through the spiracles and inhabits the trachea for several days until the vector beetle has reached a new healthy host tree. The number of dispersal L_{IV} carried by an adult beetle is a critical factor influencing the damage level of the pine wilt disease in the pine host tree (Togashi, 1985). Extraordinarily, each primary vector beetle, such as *Monochamus alternatus* in Asia, can harbor on average 15,000 and up to 280,000 nematodes in its tracheal system (Fielding and Evans, 1996). In contrast to circulative pathogens that move from gut lumen to salivary glands or ovary (Eigenbrode et al., 2018; Wei et al., 2017), and to other non-circulative pathogens that typically remain in the mouthparts (Uzest et al., 2007) and foregut of their vectors (Chen et al., 2011), PWNs merely reside, and do not multiply in the tracheal systems. However, the effects of PWN on its unique resident niche (i.e., the vector tracheal

system), and the mechanism behind the vector's competence for loading of such large numbers of PWN is still poorly understood.

Hypoxia, which occurs when oxygen supply is inadequate, is common in mammal host tissues faced with infection by pathogens and induces several adaptive responses that improve host defense by maintaining the integrity of epithelial barriers and hindering the internalization process (Zeitouni et al., 2016). Recent studies suggest a modulator role of hypoxia in various biotic interactions. For example, the parasite *Trypanasoma brucei* has evolved a way to inhibit hypoxic responses to evade the host immune response in the bloodstream (Mcgettrick et al., 2016). In contrast, a mosquito gut bacterium benefits their hosts by activating hypoxic responses improving host gut growth (Coon et al., 2017; Valzania et al., 2018). As the trachea of the adult vector beetle is packed with nematodes, reduced gas transfer ability and its consequent hypoxia are conceivable.

The insect trachea, an interconnected network of air-filled epithelial tubes characterized with optimal diameter and length, exhibits intense cycles of compression and expansion for respiration, which resembles the deflation and inflation of vertebrate lungs (Westneat et al., 2003). The tracheal volumes changed by this behavior increase the internal pressure for improvement of air convection, thus facilitating gas exchange and diffusion (Hayashi and Kondo, 2018; Westneat et al., 2003). To increase oxygen supply, the tracheal system is adapts to hypoxia by compensatory morphological and physiological changes (Harrison et al., 2018), such as extensively tracheal terminal branching (Centanin et al., 2010) and increased compression frequency of tracheal

tubes (Greenlee et al., 2013). Mechanical properties of the tracheal tubes are therefore prerequisites for regulating the tracheal geometry and compression capacity and mainly depend on a viscoelastic material surrounding tracheal lumen, called apical extracellular matrix (aECM) (Dong et al., 2014; Hayashi and Kondo, 2018; Zuo et al., 2013). In *Drosophila melanogaster*, aECMs components including serpentine, verm and dumpy affect aECM elasticity, and have been reported to mediate the tubular diameter or length, possibly by restricting apical membrane growth (Luschnig et al., 2006; Wilkin et al., 2000). A study with the American cockroach (*Periplaneta americana*) suggested that chitin structures in aECM layer are responsible for the mechanical features that enable tracheal compression and volume change during respiration (Webster et al., 2011). Similarly, high inflation of lungs is related to the mechanical forces provided by ECM components (Berg et al., 1997; Wirtz and Dobbs, 2000). In addition, hypoxia has been shown to correlate with overall aECM composition and organization of blood vessels and respiratory networks (Jang et al., 2021; Kusuma et al., 2012), implying a possible link between hypoxia and the molecular components contributing to mechanical properties of the tracheal tubes. Taken together, we hypothesize that hypoxia may be involved in the retention of PWN in vector beetle's tracheal system through the PWN exploiting mechanical properties of the vector beetle's trachea to maintain a high vector capacity in a hypoxia-regulated manner.

Here, we revealed that the number of the nematodes in the trachea is negatively correlated with the oxygen level in the tracheal system of its vector beetle, leading to

hypoxia. Both PWN loading and hypoxia enhanced the elasticity of tracheal tubes and increased the thickness of aECMs in tracheal epithelia. Based on transcriptome analysis of trachea with and without PWN, we identified aECM-related genes in the beetles and found a candidate aECM component, a resilin-like mucin protein Muc91C, the expression of which was substantially upregulated at the aECM layer after PWN loading and hypoxic treatment. *Muc91C* knockdown reduced elasticity of the tracheal tubes and aECMs thickness under hypoxic condition, indicating that *Muc91C* help regulate the aECM-related mechanical traits of the tracheal tubes. Importantly, RNAi of *Muc91C* in adult beetles significantly reduced PWN loading in trachea. These results demonstrate crucial roles of tracheal hypoxia and aECM-related tubular elasticity in improving vector competence for PWN transmission.

Results

PWN loading decreased oxygen levels in the tracheal system of vector beetle

To determine whether PWN loading reduces oxygen levels and caused hypoxia in trachea of vector beetles, we first measured the concentration of oxygen inside major thoracic tracheal tubes using an oxygen microsensor (**Figure 1A**). Radial oxygen profiles revealed a slight drop of oxygen pressure from 21kPa to 18.9kPa, respectively, when comparing pressure outside (i.e., in the ambient air) and inside the tracheal tubes of beetles without PWN. In contrast, there was a dramatic drop of oxygen pressure from 21kPa outside of tubes to 3.8kPa inside tubes when trachea was loaded with PWN (**Figure 1B**). Thus, our results showed that PWN loading induce oxygen shortage in

127 trachea.

128 We further established the correlation between oxygen level and total number of
129 nematodes in the trachea by measuring the oxygen concentration in the atrium cavity
130 of the first and largest abdominal spiracles and calculating the number of nematodes in
131 the beetle (**Figure 1A**). The partial pressure of oxygen was negatively correlated with
132 the total number of nematodes in tracheal tissue per 0.3g beetle (**Figure 1C**). The
133 curve fit to this data revealed that when the total number of nematodes reached 10,000,
134 partial pressure of oxygen in the cavity of tracheal spiracle dropped to 10 kPa (half of
135 the corresponding value in the surrounding air (usually 21 kPa), creating a mild hypoxia
136 at approximately PO_2 of 5-15 kPa. In addition, when the number of nematodes
137 increased to 44,828, the oxygen pressure dropped dramatically to 4 kPa (**Figure 1C**),
138 which is the threshold between mild and severe functional hypoxia in *Drosophila*
139 (Harrison et al., 2018). Oxygen levels in the cavity of the atrium were further compared
140 among three levels of PWN loading, differing in total number of nematodes in the
141 trachea. The tracheal systems of beetles without PWN (Null) or with light PWN loading
142 (< 10,000) had an oxygen pressure equal to that of the environment. By contrast,
143 substantial decline to approximately 4kPa of oxygen were detected in the tracheal
144 spiracle with heavy PWN loading (> 10,000). These results indicated PWN loading
145 caused oxygen loss and light or heavy PWN loading induced hypoxia or anoxia in the
146 trachea of vector beetles.

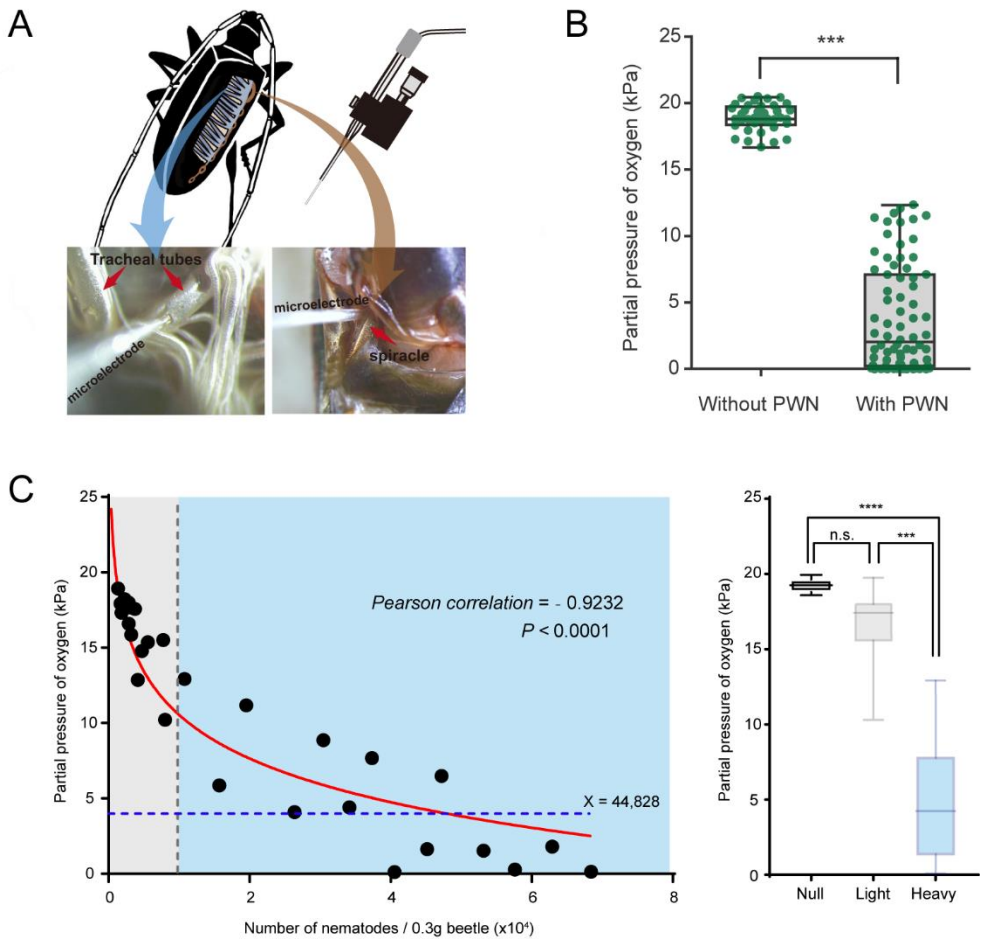

Figure 1. Negative correlation between oxygen level and PWN loading in tracheal system of *M. alternatus*. (**A**) Schematic representation of experimental setup used for microelectrode (top right) measurements inside a major trachea tube of the thorax (bottom left) and the atrium cavity of the largest spiracle (bottom right). (**B**) Partial oxygen pressure in the tracheal tubes of vector beetles with and without PWN (N = 38 and 76 tracheal tubes in 5 adults, respectively). ***$P < 0.0001$ (Mann–Whitney U test). The internal lines are medians, edges of the boxes are interquartile ranges and whiskers are minimum and maximum ranges. (**C**) The relationship between oxygen partial pressure in atrium of vector beetle (N = 5, 17 and 14 adults for null, light and heavy PWN loading) and the number of nematodes. Left panel: Fitted curve is drawn in red

158 line. The gray line, which shows 10,000 PWN, divides beetle samples into light or
159 heavy PWN loading. The blue line shows the estimated loading number of nematodes
160 when partial pressure drops to 4kPa. Right panel: Partial pressure of oxygen in atrium
161 of beetles in three different degrees of PWN loading. ***$P = 0.0001$, ****$P < 0.0001$
162 (Kruskal–Wallis nonparametric test, Dunn's multiple comparison test). The internal
163 lines are medians, edges of the boxes are interquartile ranges and whiskers are
164 minimum and maximum ranges.

165 **Nematode-induced hypoxia enhanced tracheal elasticity and thickened its apical**
166 **extracellular matrix**

167 Compared to those free of PWN, the trachea of vector beetles bearing PWN tended to
168 be rubberlike (**Figure 2-figure supplement 1A**). The total number of the nematodes in
169 the trachea correlated positively with the tracheal rubberization degree (**Figure 2-figure**
170 **supplement 1B**). Trachea with the highest rubberization degree released five times
171 more nematodes (reaching approximately 16,000 nematodes on average) compared to
172 trachea with moderate or low rubberization. Preliminary observations further showed
173 that the trachea tubes harboring PWN tended to be longer and narrower before breakage
174 under external force (**Figure 2-figure supplement 2 and Video 1 and Video 2**). This
175 relationship indicated that PWN loading influenced the mechanical properties of the
176 vector's trachea.

177 The elasticity of trachea tubes was further quantified by comparing Young's modulus
178 values of tracheal tubes among the three levels of PWN loading (null, light and heavy)

179 mentioned above. Corresponding to their higher oxygen level, Young's modulus values
180 of trachea tubes without PWN and with light PWN loading were almost two times
181 higher than the values in hypoxic trachea tubes with heavy PWN loading (**Figure 2A**).
182 Given the negative correlation between elasticity and Young's modulus values, this
183 result suggested that heavy PWN loading enhanced tracheal elasticity. To confirm the
184 influence of hypoxia on tracheal elasticity, we subjected beetles free of PWN to 1% O_2
185 for 6 h, 12 h and 24 h. Compared with that of tracheal tubes exposed to normoxia and
186 hypoxia conditions for 6h, the Young's modulus values under hypoxic treatments for
187 12h and 24 h decreased by nearly a half (**Figure 2A**). These results clearly demonstrated
188 that heavy PWN loading and its induced hypoxia enhanced tracheal elasticity.

189 Due to the correlation between mechanical properties and apical extracellular matrix
190 (aECM), we further investigated the tracheal structure with null and heavy PWN
191 loading using transmission electron microscopy. Micrographs revealed that the secreted
192 protein layer of tracheal aECM was significantly thickened by heavy PWN loading
193 (**Figure 2B and C**). However, the heavy PWN loading had no effect on the morphology
194 of the chitin layer of aECM. To examine the effect of hypoxia on tracheal aECM, we
195 treated beetles free of PWN with 1% O_2 for 6h, 12h and 24h. Electron micrographs
196 showed that the secreted protein layer of tracheal aECM under hypoxia for 12h and 24h
197 was thicker than those under normoxia and hypoxia for 6h (**Figure 2C**). Therefore, our
198 results indicated that PWN-induced hypoxia promoted the secretion of protein layers in
199 aECM in trachea. Taken together, these results suggest that the increased secretion of
200 protein layer of aECM was involved in enhanced tracheal elasticity by PWN-induced

hypoxia.

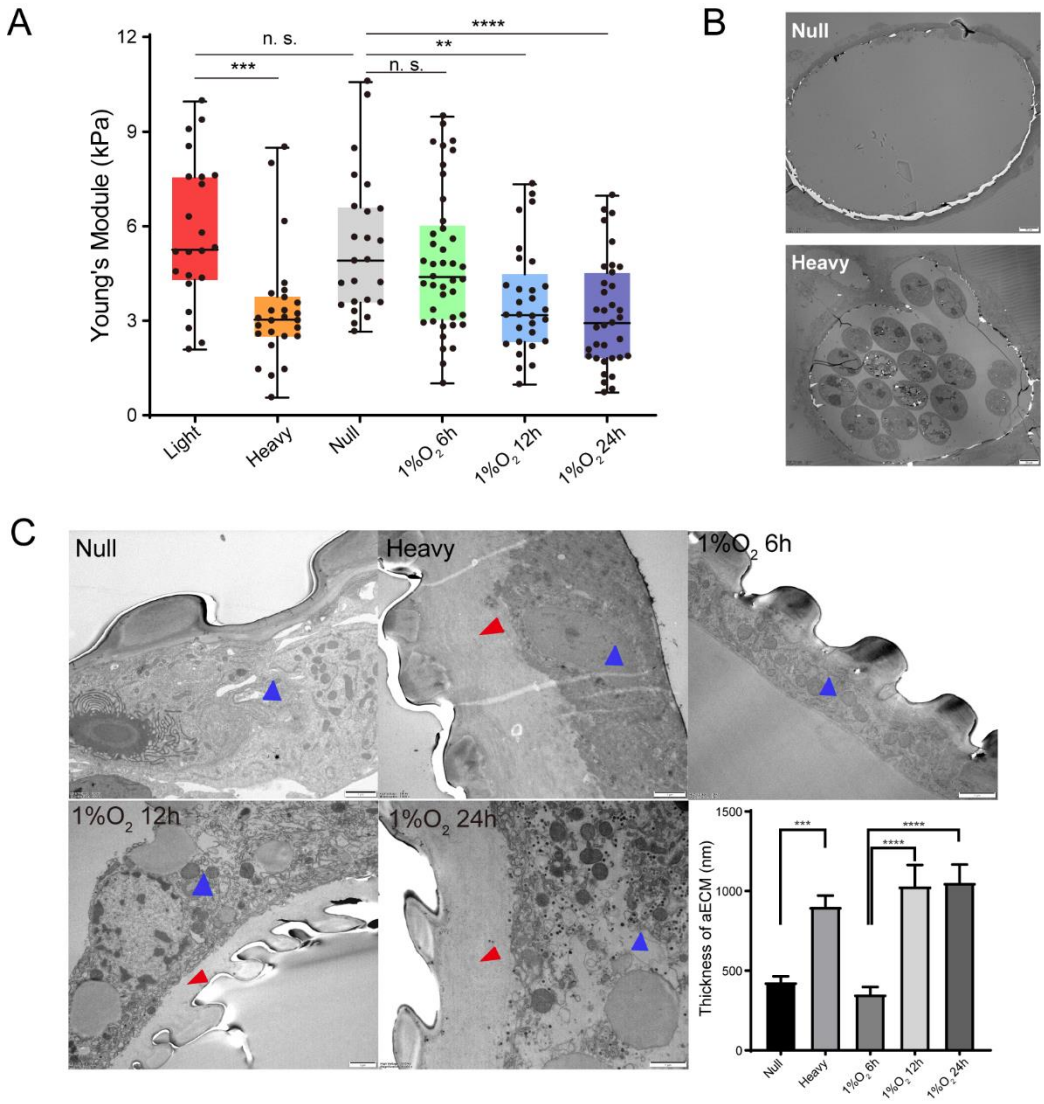

Figure 2. Effects of PWN loading and hypoxia on mechanical properties and apical extracellular matrix (aECM) of the trachea tubes of *M. alternatus*. (**A**) Calculated Young's modulus in different experimental groups according to values in tensile test in the longitudinal direction on the longest tubes linking two homolateral spiracles. Groups represent tubes from beetles without PWN (Null), light (< 10,000 nematodes), heavy (> 10,000 nematodes) PWN loading, and treated with 1% O_2 for 6h, 12h and 24h, respectively (N = 22 - 41 tracheal tubes for each treatment). $^{**}P < 0.01$, $^{***}P < 0.001$ and $^{****}P < 0.0001$ (Kruskal–Wallis nonparametric test, Dunn's multiple comparison

test). Internal lines are medians, edges of the boxes are interquartile ranges and whiskers are minimum and maximum ranges. (**B** and **C**) Transmission electron micrographs (TEMs) for axial views of the longest tracheal tubes. (**B**) Representative images were shown for global view of tracheal tubes without (Null) and with heavy PWN loading. Bars, 20μm. Experiments were performed at least three times. (**C**) Electron microscopy images showed the thickened tracheal aECM (red arrow) between the chitin layer (taenidial ridges) and the body of tracheal cell (blue arrow) after different treatments (without PWN, i.e. Null, heavy PWN, and 1% O_2 for 6h, 12h and 24h, respectively). Bars, 1μm. The right bottom panel shows the statistical data of the thickness of aECM corresponding to TEMs. Data were measured in 6 tracheal tubes of 3 adults for each treatment. ***$P < 0.001$ and ****$P < 0.0001$ (Kruskal–Wallis nonparametric test, Dunn's multiple comparison test). Data are represented as mean ± SEM.

PWN loading caused significant upregulation of Muc91C responsible for the thickened aECM layer in trachea

To confirm the role of proteins to the enhanced tracheal elasticity, we compared the tracheal transcriptomes between PWN free and heavily PWN loaded beetles and discovered 916 differentially expressed genes (DEGs). Out of these, 251 DEGs were identified as aECM-related genes (**Figure 3A**). Overall, the altered transcript profiles suggested dramatic epithelium reorganization in tracheal tubes of vector beetles after PWN loading. We then chose 45 genes related to mechanical properties to further scrutinize for their expression (**Figure 3B**). We examined chitinases, chitin synthases

232 and chitin deacetylases, which are involved in chitin catabolic processes, biosynthetic
233 processes, and arrangement, respectively (Dong and Hayashi, 2015). The up or down
234 regulated pattern in the expression of these transcripts suggested a chitin metabolic
235 equilibrium, which was consistent with the unchanged chitin layer among beetles with
236 heavy PWN loading shown in TEMs (**Figure 2C**). Our gene list also included those
237 genes functioning as aECM regulators. For example, Metalloproteinases are
238 proteinases that cleave proteins in the extracellular matrix (Glasheen et al., 2010).
239 Cadherins, integrins, lachesin and dumpy are transmembrane proteins participating in
240 signal transduction between aECM and tracheal cells (Llimargas et al., 2004; Öztürk-
241 Çolak et al., 2016; Wilkin et al., 2000). The changed expression of these transcripts
242 after heavy PWN loading indicated altered regulatory cascades of aECM. We finally
243 investigated the expression of the non-chitin structural components including mucins,
244 collagens and laminin. Negatively regulated transcripts of collagens in heavy loading
245 PWN samples and the location of laminin in basal lamina of tracheal cells (Dai et al.,
246 2018) suggest they were not responsible for thickening the aECM layer in our
247 observations (**Figure 2C**). Therefore, the genes encoding for the mucin family, a group
248 of large glycosylated macromolecules, are possible candidate genes contributing to the
249 elasticity of trachea in our study, because their location and upregulation directly
250 corresponded to the observed thickened non-chitin layer in aECMs visible in electron
251 microscopy (**Figure 2C**). To investigate possible correlation between tracheal
252 development at metamorphosis and after PWN loading, we further scrutinized the
253 expression of the 45 aECM genes in tracheal tubes after one day, three days, five days

and seven days post eclosion, using RNA-seq data in a published study (Tang et al., 2022). All genes were downregulated between day 5 and day 7 post adult eclosion (**Figure 3-figure supplement 1**). Therefore, tracheal system of vector beetles responded to loading nematodes despite the completion of tracheal development. For *Muc91C* specifically, its expression was 2-fold upregulated three days after eclosion but was downregulated during the later stages post eclosion. However, PWN loading resulted in a 7-fold increase of *Muc91C* expression, a higher fold-change than that during tracheal development.

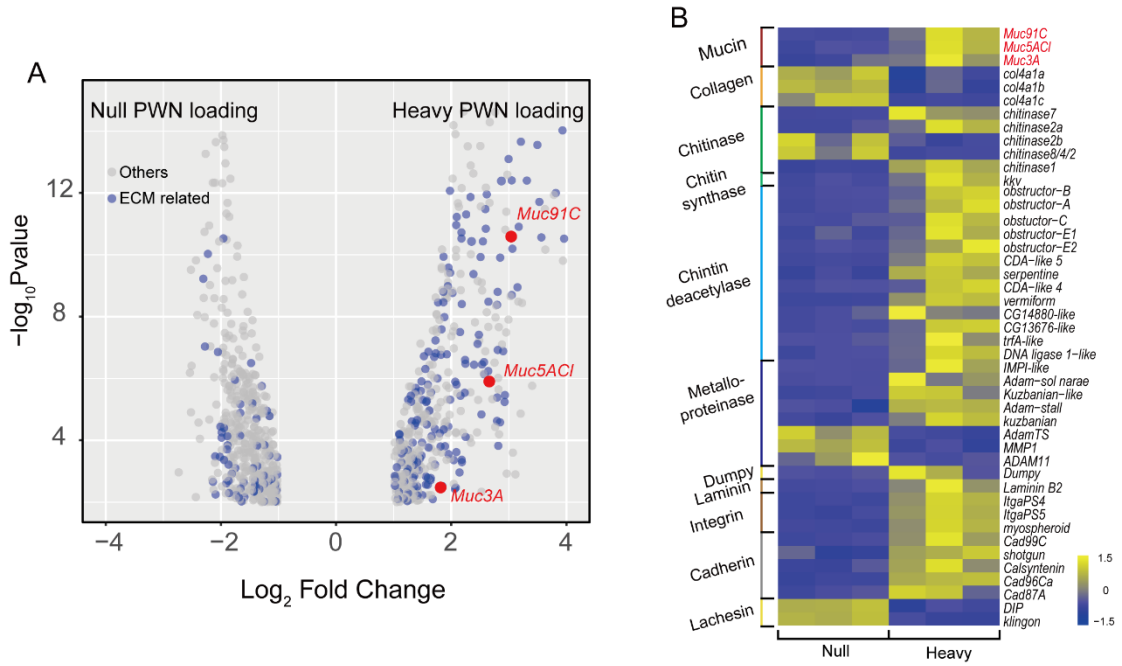

Figure 3. Transcriptome analysis showed changed expression pattern of aECMs-related genes in trachea treat with PWN. (**A**) Volcano plot of RNA-seq data from trachea of beetles with and without PWN. Grey dots indicate all DEGs, and blue dots indicate aECM-related DEGs. The red dots indicate the three mucins. (**B**) Heat map of differential expressed genes related to mechanical property of tracheal tubes of beetles with and without PWN. The red font indicates the three mucins.

269 Among the three mucin genes, *Muc91C* had the highest increase in expression after
270 PWN loading, increasing more than seven folds (log2FC = 2.43), higher than the other
271 two genes (**Figure 3A**). Next, we independently validated our RNA-seq results by
272 repeating the experiment using new individuals and quantifying expression using
273 reverse-transcription qPCR (RT-qPCR) for the genes that belong to the mucin family.
274 In contrast to the other two mucin genes, the abundance of *Muc91C* transcripts
275 positively correlated with the level of PWN loading in trachea (**Figure 4A**). Compared
276 to that of trachea without PWN, the expression level of the *Muc91C* gene increased
277 five-fold in trachea with heavy PWN loading. To test the effect of hypoxia on *Muc91C*,
278 *Muc5ACl* and *Muc3A*, gene expression levels were measured after exposure of beetles
279 under 1% O2 for 6h, 12h and 24h. Hypoxia treatment of 12h caused significant
280 upregulation of *Muc91C* in trachea (**Figure 4B**). To exclude the influence of related
281 tissues, we examined the tissue specificity of *Muc91C* in tracheal tubes, flight muscle
282 and midgut. Compared to fight muscle and midgut, *Muc91C* expression was mostly
283 highly expressed in the trachea of adult beetles with or without PWN loading. Heavy
284 PWN loading significantly increased *Muc91C* expression in all tested organs (**Figure**
285 **4C**), implying systematic hypoxia in beetles with heavy loading. We also further
286 confirmed the protein levels of *Muc91C* in tracheal tubes with null, light and heavy
287 PWN loading by Western blot analysis. The PWN loading enhanced Muc91C in a
288 nematode number-dependent manner (**Figure 4D**), similar with the tendency of oxygen
289 loss in tubes with PWN (**Figure 2C**). These results indicated that heavy PWN loading
290 in beetles' trachea stimulates the expression of Muc91C via inducing hypoxia. We

291 further investigated the localization of Muc91C in tracheal tubes through
292 immunohistochemistry analysis. Strong signals for Muc91C were detected beneath the
293 layer of taenidial folds (**Figure 4E**) and above the apical membrane of the tracheal cell
294 (**Figure 4F**) forming a continuously layer in tracheal tubes with heavy PWN, whereas
295 slight fluorescence signal was observed in tracheal tubes without PWN. Thus, this result
296 demonstrated that Muc91C is the component of the PWN-thickened aECM layer
297 showed in TEM.

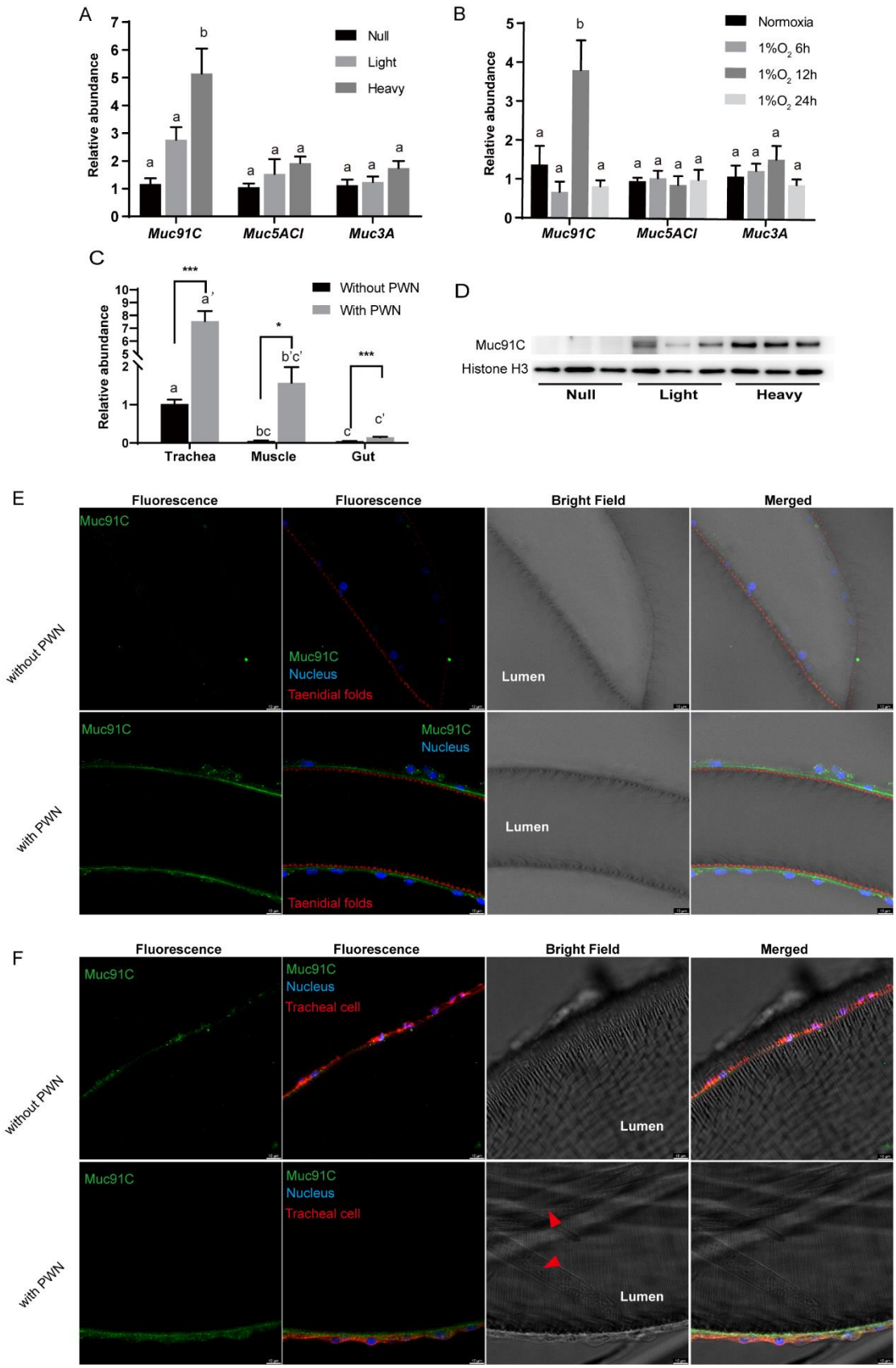

298

299 **Figure 4. Heavy PWN loading and hypoxia enhance Muc91C expression at the**

300 **aECM layer in tracheal tubes.** (**A**) Relative RNA abundance of three genes belonging

301 to mucin family in trachea of beetles with null, light (< 10,000 nematodes) or heavy (>
302 10,000 nematodes) PWN loading. Data are represented as mean ± SEM. Columns
303 labeled with different letters indicate statistically significant differences in mean
304 relative abundance (N = 7-8 for each gene, one-way ANOVA with Tukey's multiple
305 comparisons, P = 0.0003, 0.1992, 0.1353 for *Muc91C*, *Muc5ACl* and *Muc3A*,
306 respectively). (**B**) Relative RNA abundance of three genes belonging to mucin family
307 in trachea of beetles under normoxia or 1% O_2 for 6h, 12h, or 24h. Data are represented
308 as mean ± SEM. Columns labeled with different letters indicate statistically significant
309 differences in mean relative abundance (N = 5 for each gene, one-way ANOVA with
310 Tukey's multiple comparisons, P = 0.0009, 0.9389, 0.3662 for *Muc91C*, *Muc5ACl* and
311 *Muc3A*, respectively). (**C**) Relative RNA abundance of *Muc91C* in tracheal tubes, flight
312 muscle and midgut of beetles with null or with heavy PWN loading. Data are
313 represented as mean ± SEM. *P < 0.05, ***P < 0.001 (N = 4, Mann-Whitney
314 nonparametric test). Columns labeled with different letters indicate statistically
315 significant differences in mean relative abundance (N = 4, one-way ANOVA with
316 Tukey's multiple comparisons, P < 0.0001 for beetles with or without PWN). (**D**) The
317 protein level of Muc91C in tracheal tube with null, light, heavy PWN. Histone H3 is
318 used as internal control. Three biological replicates of each treatment are shown. (**E**)
319 and (**F**) Immunostaining images of tracheal tube with Null and Heavy PWN showed
320 the localization of Muc91C (Green), taenidial folds (Red in **E**), tracheal cell body (Red
321 in **F**) and nuclei (Blue). Bars, 10μm. Experiments were performed at least three times.
322 The red arrowhead in bright field image showed residual PWN in the tracheal tube.

323 ***Muc91C* contributes to hypoxia-enhanced trachea elasticity and promote PWN**
324 **loading**

325 In order to determine whether increased Muc91C contribute to the tracheal
326 elasticity, we investigate its gene structure and revealed that *Muc91C* encoded a resilin-
327 like protein (Andersen, 2010), dominated by two long regions containing a series of
328 short repeat motifs (**Figure 5**). Seventeen A repeats, with the consensus sequence
329 PSSSYGAPA(S) were located in the N-terminal region. Additionally, eleven B repeats,
330 with the consensus sequence GGYSSGGN, were located in the C-terminal region. As
331 the only identified MaMuc91C homolog in insects, DmMuc91C was classified as a
332 resilin-like protein (Andersen, 2010). In addition, a BLASTX search of MaMuc91C
333 against Flybase revealed its similarity not only to DmMuc91C (CG7709-PB) but also
334 to functional DmPro-resilin (CG15920-PA). Using DmPro-resilin and resilin-like
335 DmMuc91C as query sequences in turn, we further characterized 17 resilin-related
336 genes in the tracheal transcriptome of the PWN vector beetle and in the genomes of
337 other insects. Phylogenetic analysis revealed that MaMuc91C and six proteins from
338 other insects were assigned to clade I, which share repeat A motif with a consensus
339 sequence of PS(Q)SSYGAP(A)S. Importantly, sequence in clade I shared two features
340 with pro-resilin proteins. First, the glycine and proline residues, indicating its long-
341 range elasticity. Second, a tyrosine residue, which presumably facilitates the formation
342 of dityrosine crosslinks after secretion from the epidermal cells. However, clade I
343 lacked the chitin binding R&R Consensus sequence, a defining feature of true pro-
344 resilin. Thus, these proteins were classified as resilin-like proteins. Based on the PTS

domain and O-glycosylation sites (Zhao et al., 2020), we found that all the proteins in clade I (**Figure 5**) belonged to the mucin family and may be homologues of Muc91C, given their similarity with DmMuc91C. The other six resilin-related proteins were true pro-resilins and clustered into clade II, in which repeat A motifs were highly variable and all sequences contained the chitin binding R&R Consensus. No pro-resilin homologue was identified in tracheal transcriptome of *M. alterantus*. Regardless of the existence of R&R Consensus sequence, repeat A consensus in both pro-reslins and Muc91C are known to directly regulate long-range elasticity. Previous studies have shown that synthetic peptide chains containing either the A-repeat-containing region from DmPro-resilin or a series of A repeats from the AgaMuc91C (AGAP002367-PA) form rubberlike elastic materials (Elvin et al., 2005; Lyons et al., 2007; Nairn et al., 2008). In addition, phylogenetic analysis based on *M. alternatus.* and other insect species' mucin sequences showed that Muc91C proteins were clustered into a separate lineage (**Figure 5-figure supplement 1**). We therefore deduced that *MaMuc91C* encodes an insect-originated resilin-like protein and has a potential role in providing long-range elasticity.

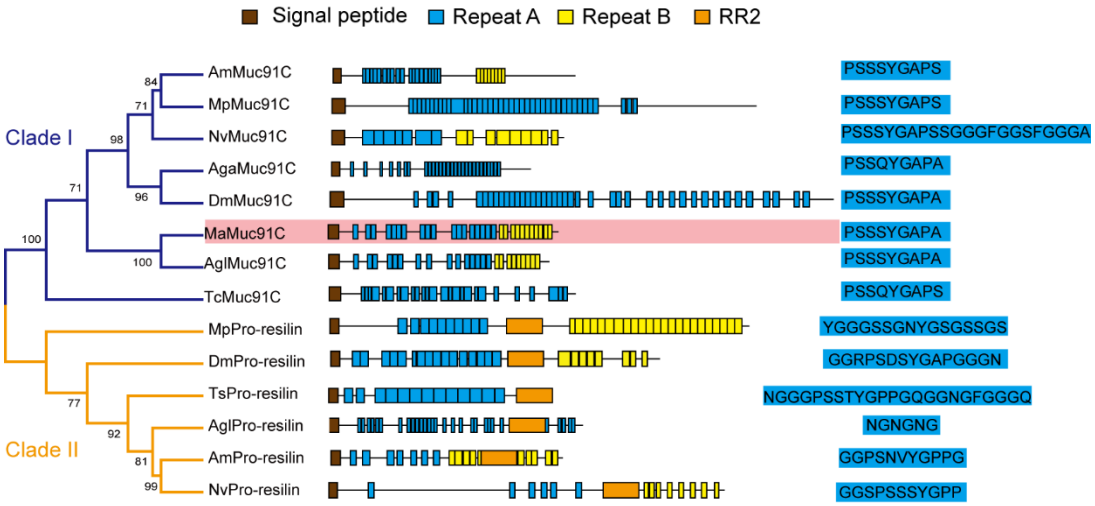

362 **Figure 5. Phylogenetic relationship among resilin-related proteins in insects.** The
363 phylogenetic analysis was performed using the full-length amino acid sequences of
364 representative resilin-related proteins. Am, Apis melifera. Mp, Myzus persicae. Nv,
365 Nasonia vitripennis. Aga, Anopheles gambiae. Dm, Drosophila melanogaster. Ma,
366 *Monochamus alternatus.* Agl, Anoplophora glabripennis. TC, Tribolium castaneum. The blue and
367 yellow branches represent Muc91C (Clade I) and Pro-resilin (Clade II), respectively.
368 The domain architectures are listed at the middle panel. Brown boxes indicate signal
369 peptide. Blue boxes indicate repeats A. Yellow boxes indicate repeats B. Orange boxes
370 indicate RR2. The consensus sequences of repeats A are listed at the right panel.
371 MaMuc91C is highlighted in pink.

372 We further verified the key role of *Muc91C* in determining the thickness of aECM
373 and its related elasticity under hypoxia condition. Firstly, we used TEM to observe the
374 substructure of tracheal tubes treated with 1% O_2 for 12h, after performing gene
375 knockdown of *Muc91C* in adult beetles. RNAi knockdown of *Muc91C* in adult beetles
376 within two days after eclosion resulted in a 77.5% decrease in *Muc91C* mRNA levels
377 and has no detrimental influence on adult survival (**Figure 6-figure supplement 1A &**
378 **1B**). Compared to ds*GFP*-injected beetles, the thickness of aECM layers in tracheal
379 tubes were substantially reduced in ds*Muc91C*-injected beetles (**Figure 6A**). Next, we
380 measured Young's modulus values of trachea tubes treated with 1% O_2 for 12h after
381 dsRNA injection. Compared to the ds*GFP* control, the Young's modulus values of
382 tracheal tubes were significantly increased in the ds*Muc91C* samples, indicating their
383 decreased elasticity after *Muc91C* knockdown (**Figure 6B**). Therefore, the enhanced

384 tracheal elasticity induced by hypoxia relies on the expression of *Muc91C*.

385 To further confirm the role of *Muc91C*-induced elasticity in PWN loading, we carried
386 out *Muc91C* knockdown in adult beetles and subsequently inoculated beetles with
387 PWN. Injection of *dsGFP* and *dsMuc91C* resulted in similar proportions of death before
388 dissection for PWN counting (**Figure 6-figure supplement 1C**). Compared to beetles
389 injected with ds*GFP*, the number of nematodes in beetles injected with ds*Muc91C* was
390 reduced by 50%, and the total number of nematodes in these beetles' trachea reaching
391 less than 10,000 (**Figure 6C**). Collectively, *Muc91C* was essential to promote heavy
392 PWN loading by promoting tracheal elasticity during hypoxia.

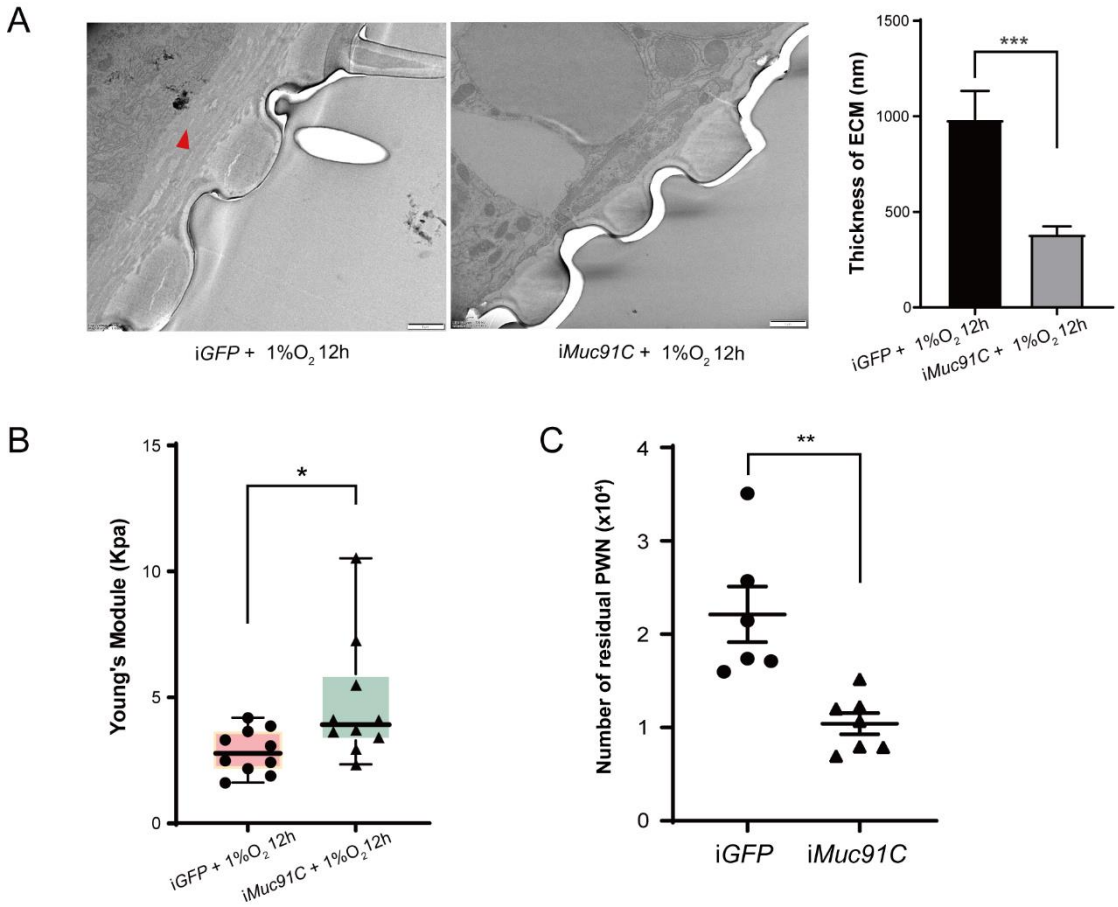

393

394 **Figure 6. The role of *Muc91C* in tracheal elasticity and PWN loading.** (**A**) Electron
395 microscopy images showed the thickened tracheal aECM (red arrow) under 1% O_2 for

12h after ds*GFP* or ds*Muc91C* injection. Bars, 1μm. The right panel shows the statistical data of the thickness of aECM corresponding to TEMs. Data were measured in 6 tracheal tubes of 3 adults for each treatment. ***$P < 0.001$ (Mann-Whitney nonparametric test). Data are represented as mean ± SEM. (**B**) Young's modulus of trachea treated 1% O_2 for 12h after ds*GFP* or ds*Muc91C* injection (N = 10 tracheal tubes for each treatment). *$P < 0.05$ (Mann-Whitney nonparametric test). The internal lines are medians, edges of the boxes are interquartile ranges and whiskers are ranges. (**C**) Number of residual PWNs released from every 0.3g beetle incubated with PWN (N = 6 and 7 adults, respectively). ds*GFP* or ds*Muc91c* is injected before incubation. **$P < 0.01$ (Student's t-test, unpaired and two-tailed). Data are represented as mean ± SEM.

Discussion

Vector competence is important for vector-borne pathogens' transmission, but the underlying mechanism remains largely unexplored. Here, we demonstrate one of strategies that PWN utilizes to maintain itself in its vector by modulating the vector beetle's hypoxia responses. This strategy helps the nematode to reach high numbers even in a single vector beetle and may consequently promote the successful spread, establishment and outbreak of pine wilt disease. Mechanically, we propose that PWN's loading process in vector beetles follows a positive feedback loop (**Figure 7**). First, continuous entering of nematodes into trachea decreases oxygen levels, resulting in hypoxia, which in turn increases the elasticity of tracheal tubes by upregulating *Muc91C*. The more elastic tube structure, in turn, allows more nematodes to reside in

the lumen until maximum elasticity is reached, resulting in decreased gas transfer due to physical blocking caused by nematodes. Finally, the resulting high level of CO_2 drives nematodes away from the trachea (Wu et al., 2019). Thus, the nematodes strategically manage their loading and departure from the vector by manipulating oxygen supply in the vectors' trachea.

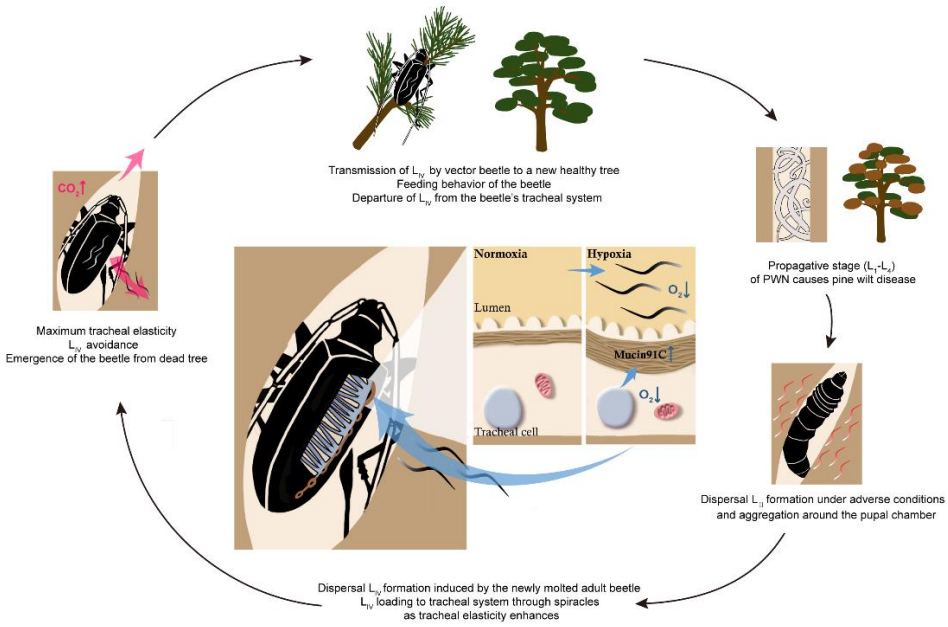

Figure 7. Schematic diagram of the feedback regulation of PWN loading through O_2 and CO_2 level in the tracheal system of *M. alternatus*. When L_{IV} dispersal nematodes continuously enter the vector beetle through spiracles, the consequent hypoxia enhances the elasticity of tracheal tubes by upregulating *Muc91C*. The more elastic tube structure, in turn, allows more nematodes to reside in the lumen. When tracheal tubes reach to their maximum elasticity, nematodes influence gas exchange of beetles and the resultant high level of CO_2 drives nematodes away from the trachea.

Hypoxia occurs universally across living organisms and plays multiple roles in hosts infected by pathogens. For instance, a protozoan parasite *Leishmania donovani* induces

432 inflammatory hypoxia to limit the capacity of the host's myeloid cells to kill the parasite
433 (Hammami et al., 2017). Some commensal gut microbiota maintains epithelial hypoxia
434 to limit the growth of enteric pathogens in the gut lumen of chicks (Litvak et al., 2019).
435 However, hypoxia in pathogen-vector relationships has long been a neglected research
436 topic. Our study shows that retention of nematodes caused hypoxia in tracheal tubes of
437 vector beetles, providing empirical evidence for a previous hypothesis that the heavy
438 PWN loading hinders the gas exchange of the beetle (Togashi and Sekizuka, 1982).
439 Such hypoxia induced by PWN loading improved the vector's tracheal capacity to
440 harbor PWN. The correlation between hypoxia and vector competence can be
441 extrapolate to the interaction between circulative pathogens and their vectors, because
442 their migration, replication or propagation processes inside vectors may also increase
443 oxygen demands and result in hypoxia.

444 Mechanical properties of tracheal tube are critical to luminal volume by regulating
445 tubular size (Dong et al., 2014) and the dynamic volume changes during tracheal
446 compression and expansion to increase the internal pressure for air convection and
447 gases exchange, thus facilitating oxygen diffusion (Westneat et al., 2003). Our results
448 show that after heavy PWN loading or hypoxic treatment, the thickness of ECM in the
449 tracheal tubes of the vector beetle are remarkably enhanced. Regardless of an intricate
450 relationship between ECM thickness and tubular diameter, the thickened ECM layer
451 results in more elastic tubes that qualify a robust compression. Such improvement of
452 compression capacity via tubular elasticity might be response to acute hypoxia or PWN
453 loading, different from the chronic adaption that involve tracheal diametric expansion

454 in *Drosophila* larvae incubated under constant hypoxic condition for generations
455 (Henry and Harrison, 2004). In the PWN-beetle system, heavy PWN loading occupies
456 luminal volume needed by tracheal ventilation for the beetle's regular respiration or
457 intensive respiration during dispersal flight in the search of suitable host pine trees. The
458 enhanced tracheal elasticity adapts vector insects to hypoxic stress allowing more
459 oxygen inhalation and provides adequate lumen volume to carry large numbers of
460 nematodes. Therefore, altered mechanical properties of the beetles' trachea after PWN
461 loading likely maintains a balance between a limited fitness cost to beetles and high
462 vector competence for effective transmission of PWN.

463 Along with enhanced tracheal elasticity in the vector beetle, our study also found
464 remarkable global expression changes of aECM genes after PWN loading regardless of
465 the termination of tracheal differentiation and maturation within the first five days after
466 eclosion. For example, metalloproteinases degrading old cuticle and promoting apical
467 membrane expansion (Glasheen et al., 2010), cadherins and integrins participating in
468 signal transduction between aECM and tracheal cells (Hayashi and Kondo, 2018;
469 Öztürk-Çolak et al., 2016) are significantly upregulated after heavy PWN loading. This
470 result suggests that PWN loading causes dramatic epithelium reorganization in tracheal
471 tubes of vector beetles. Therefore, our study provide an example that the tracheal
472 system is able to immediately respond to the environment by epithelium reorganization
473 through changed aECM components. Although aECM is crucial to determine
474 mechanical properties of tubular organs including trachea, the role of its molecular
475 components remains largely unknown. Using gene manipulation, we further identified

Muc91C, which encodes a resilin-like protein in aECM, as the key component responsible for the thickening of non-chitin aECM layer and the improved tracheal elasticity. However, due to incomplete reduced elasticity under hypoxic condition in ds*Muc91C*-injected beetles, other tracheal cellular components such as proteins embedded in the membrane may also regulate tracheal elasticity. Structurally, Muc91C in *M. alternatus* contains two types of repeat motifs but lacks chitin-binding RR2, a consensus sequence in resilin monomers (pro-resilins) (Michels et al., 2016), suggesting that its elasticity trait resides in the repeat motifs. Consistent with the absence of pro-resilin in the tracheal tubes of vector beetles, *Drosophilia* larval foregut is devoid of pro-resilin, but contains resilin-like Cpr56F (Lerch et al., 2020). Collectively, these examples suggest that resilin-like proteins are employed instead of resilin monomers in deformation of various cuticle-free organs. Interestingly, remarkably upregulated *Muc91C* expression were also detected in flight muscles and midgut of beetles with heavy PWN loading. Because mucins are highly glycosylated macromolecule proteins, protecting cells against microbial infection (Martens et al., 2018), higher systematic *Muc91C* level in various tissues may contribute to maintaining the integrity of mucosal barriers to alleviate the detrimental effects of nematodes invasion, such as increased ROS reported in previous studies (Zhou et al., 2018).

The present study found that hypoxia promotes tracheal elasticity by upregulating the expression of *Muc91C*, suggesting that *Muc91C* is related to hypoxia adaptation. Similarly, significant upregulated expression of pro-resilin has been demonstrated in an intertidal crustacean, the copepod *Tigriopus californicus*, when exposed to extremely

low oxygen levels (Graham and Barreto, 2019). Therefore, the sensitivity of gene expression of aECM components in epithelial tissues to hypoxia is likely a pervasive phenomenon in arthropods. Clustering into a separate lineage in the Mucin phylogenetic tree (**Figure 5-figure supplement 1**), all insect Muc91C proteins investigated in this study had no human homologues and were only distantly related to other mucins, suggesting their independent evolutionary origin in insects. This result is consistent with a previous study reporting that Muc91C is the only mucin structurally similar to pro-resilins among 23 mucins and mucin-related proteins in *D. melanogaster* (Syed et al., 2008). In Asian longhorned beetles (*Anoplophora glabripennis*), for instance, AgMuc91C has 84% sequence similarity with *MaMuc91C* (**Figure 5**). Therefore, further examination of *Muc91C* expression patterns and its responses to hypoxia in other pine sawyer beetles closely related to our study species, such as *Monochamus saltuarius* can help to assess the role of *Muc91C* in facilitating heavy PWN loading and thus to pine wood disease. Overall, our study provides evidence of exploitation of hypoxia-enhanced tracheal elasticity by a plant parasitic nematode to improve vector competence in this unique pathogen-vector system and offers new insights for the development of novel targets to control the pine wilt disease.

Materials and methods

Collection and rearing of nematodes and beetles

Mature larvae of sawyer beetles (*M. alternatus*) were collected from dead pine trees in the Fuyang area, Hangzhou City, Zhejiang Province, and reared in an incubator (26°C,

519 humidity 35%) until they pupated or for seven days after eclosion. *B.xylophilus* were
520 originally acquired from infected trees in Shannxi Province and maintained with
521 *Botrytis cinerea* in potato dextrose agar (BD, 213400) plates at 25°C for generations
522 until used in the experiments.

523 **Nematode loading, tracheal dissections, and nematode quantification**

524 50ml Erlenmeyer flasks containing *B. cinerea* growing in autoclaved (121°C, 30min)
525 barley medium (10g barley in 15ml water) for two weeks at 25°C, were inoculated with
526 1,000 propagative nematodes. After the nematodes had fed for five days, autoclaved
527 pine wood sawdust layer was spread on top of the barley layer of the rearing flasks and
528 cultured in 4°C for another two weeks. When the color of the pupae's eyes turned dark,
529 they were put on the nematode-infected sawdust layer until six days after eclosion.
530 Emerged adult beetles were dissected by ventral filleting, and the tracheal tubes located
531 on both sides of the thorax were dissected and carefully deprived of surrounded muscle
532 under a stereomicroscope (Olympus SZX16, Japan). The excised tracheal tubes and the
533 left part of the body were washed in PBST (Solarbio, P1033) to irrigate the nematodes
534 and presence of nematode was confirmed under a stereomicroscope (Olympus SZX16,
535 Japan). The total number of isolated nematodes per beetle were counted in plates with
536 an inverted microscope (Olympus CKX41, Japan).

537 **Measurement of oxygen concentrations**

538 The measurement of oxygen concentrations followed previous studies with

539 modifications (Brune et al., 1995; Pettersen et al., 2005). The Oxygen Microsensors
540 with tip diameters of 25 μm (Unisense OX-25-905248, Denmark) and 100 μm
541 (Unisense OX-100-909667, Denmark), respectively, were used to penetrate into trachea
542 tubes (which are visible after ventral filleting and gut removal) and poke into the atrium
543 cavity of the largest spiracles located on both sides of the thorax. This protocol was
544 used for beetles without or with nematodes to obtain high-resolution profiles of oxygen
545 concentrations. Prior to use, the electrodes of the microsensors were polarized overnight
546 in deionized and continuously aerated water. Calibration was carried out before and
547 after each experiment and was done by measuring the current when the microelectrode
548 was placed in water saturated with air (21kPa O_2) and measuring the background
549 current in 1% Na_2SO_3 (0kPa O_2). The values were measured with an amperemeter
550 (Unisense oximeter-5591, Denmark) connected to a computer with a software
551 SensorTrace Logger (Unisense, Denmark). Oxygen microsensor was fixed on a
552 micromanipulator. Once placed into tracheal tubes and poking into the atrium cavity
553 under a stereomicroscope, the microsensor was paused for at least 20s to ensure
554 sufficient data collection. The microsensor was then pulled out and recording was
555 continued for 15s to record values of the ambient air. To take into account temperature
556 derived fluctuation in saturated oxygen concentration of different tests, we converted
557 the concentrations to its corresponding partial pressure, and the average partial pressure
558 of oxygen during the 20s inside the trachea was calculated as the final data.

559 **Hypoxic treatment**

560 Hypoxic treatment was performed in a hypoxic chamber (FLYDWC-50; Fenglei Co.,
561 Ltd, China) placed in an artificial box to automatically control the ambient temperature,
562 air flow and pressure of oxygen (PO_2). Adult beetles without nematodes were placed in
563 the ventilated chamber, in which air flow was balanced with pure nitrogen to achieve
564 the required 1% O_2. The adult beetles were maintained in the chamber for 6h, 12h, or
565 24h at 25 ± 1 °C in the dark.

566 **Measurement of rubber-like degree**

567 Adult beetles post 6 days after eclosion were dissected by ventral filleting, and the
568 morphological trait of thoracic tracheal tubes without and with heavy PWN were
569 observed under a stereomicroscope (Olympus SZX16, Japan). Tracheal tube which lost
570 its original orange metallic luster and become pink and leathery are defined as a rubber-
571 like tube. The number of the rubber-like tubes and the total number of thoracic tracheal
572 tubes oxygenate to flight muscle were counted and the rubberization degrees were set
573 into three degrees according to the ratio of the former two values (I, none; II, less than
574 50% rubber-like tubes; III, 50%~100% rubber-like tubes). Then, the number of PWN
575 harbored in beetles were counted.

576 **Measurement of mechanical properties with tensile testing**

577 The two longest tracheal tubes linking the largest spiracle on both sides of the thorax
578 and the spiracle basal to the head of the beetle were dissected as mentioned above and

579 were maintained at room temperature (RT) in PBS (Solarbio, P1020). According to a
580 previous study on muscle fibers (Kaiser et al., 2019), tensile testing was performed with
581 a micromechanical system (Aurora Scientific, Ontario, Canada) equipped with a length
582 controller (322C), a 10mN force transducer (405A), and dynamic control software suite
583 DMC (ASI 600A). The measurements were performed inside a bath with PBS at room
584 temperature. The dissected tracheal tubes were tied to the fixed hooks at the ends of
585 length controller and force transducer using nylon fibers. Prior to testing, the
586 unstretched lengths (L_0) and radius (r) of the tubes were measured with caliper under
587 an inverted microscope (Olympus CKX41, Japan). All samples were tested at a constant
588 strain rate of 10% L_0/ 3 sec until failure or 2 × L_0. The stiffness of the tubes was
589 characterized by the Young's modulus (E) determined from the linear region of the
590 stress-strain curve, usually between 30% and 80% strain, using the equation of $E = \{(F$
591 $/ \pi r^2) / (\Delta L/ L_0)\}$.

592 **Transmission electron microscopy of the tracheal tubes**

593 The two longest tracheal tubes linking the largest spiracle on both sides of the thorax
594 and the spiracle basal to head of the beetle were dissected and instantly fixed with 2.5%
595 (vol/vol) glutaraldehyde (Coolaber, SL1790) and 4% (vol/vol) paraformaldehyde
596 (Solarbio, P1112) with Phosphate Buffer (PB) (0.1 M, pH 7.4) (Macklin, H885798).
597 The samples were then washed four times in PB and then tubes were postfixed with 1%
598 (wt/vol) osmium tetraoxide in PB for 2 h at 4 °C, dehydrated through a graded ethanol
599 series (30, 50, 70, 80, 90, 100%, 100%, 7min each) into pure acetone (2×10min).

600 Samples were infiltrated in graded mixtures (3:1, 1:1, 1:3) of acetone and SPI-PON812
601 resin (16.2 g SPI-PON812, 10 g DDSA and 8.9 g NMA), and then changed to pure resin.
602 Finally, tubes were embedded in pure resin with 1.5% BDMA and polymerized for 12h
603 at 45°C, 48 h at 60°C. The ultrathin sections (70nm thick) were sectioned with
604 microtome (Leica EM UC6, Germany), double-stained by uranyl acetate and lead
605 citrate, and examined by a transmission electron microscope (FEI Tecnai Spirit120kV,
606 Oregon, USA).

607 **RNA-seq and Transcriptome analysis**

608 Each sample for RNA-seq was prepared by combining four individual beetles (two
609 females and two males, six days after emergence) for one library construction. The two
610 libraries included trachea of sawyer beetles with and without PWN. Tracheal tubes were
611 extirpated, washed with PBS to remove the nematodes, and immediately flash frozen
612 with Trizol (Invitrogen,15596018) and stored in -80°C before use. Total RNA was
613 isolated from the frozen samples using Trizol reagent according to the manufacturer's
614 protocol. mRNA was purified with a Dynabeads mRNA purification kit (Invitrogen,
615 61012). PolyA containing mRNAs was enriched with oligo (dT) magnetic beads (NEB,
616 S1419S), fragmented with RNA fragmentation reagent, and subjected to the following
617 procedure: first- and second-strand cDNA synthesis, purification, end repair, single-
618 nucleotide addition, ligation of adapters, purification of ligated products, and PCR
619 amplification for cDNA template enrichment. The RNA-seq library preparation kit for
620 whole transcriptome discovery (compatible with Illumina, San Diego, California, USA)

621 was used (Illumina Whole-Genome Gene Expression BeadChips). The 320 - 420bp
622 products were purified with the MiniElute gel extraction kit (Qiagen, Hilden, Germany)
623 and sequenced with the Illumina novaseq 6000 platform at Biomarker Technologies Co,
624 LTD.

625 **Identification and analysis of aECM-related genes from the transcriptome and**
626 **phylogenetic analysis**

627 Using the SignalP 3.0 (http://www.cbs.dtu.dk/services/SignalP), we predicted secreted
628 proteins in DEGs, based on the presence and extension of signal peptides. The retrieved
629 proteins were manually confirmed by Nr, GO, KO annotations, and using pfam and a
630 BlastX search against the amino acid sequences of known ECM-related genes from
631 flybase (http://flybase.org/). Transmembrane domains were analyzed by TMHMM
632 server v. 2.0 (http://www.cbs.dtu.dk/services/TMHMM/). The RR2 Consensus
633 sequences were predicted using the cuticleDB website
634 (http://bioinformatics2.biol.uoa.gr/cuticleDB/index.jsp). The O-glycosylation sites of
635 mucin proteins were determined by NetOGlyc 4.0
636 (www.cbs.dtu.dk/services/NetOGlyc). To verify the classification of resilin-related
637 proteins and other mucin proteins, phylogenetic analysis was performed using the full-
638 length amino acid sequences of representative proteins from other species retrieved
639 from the GenBank database. Multiple alignments of the amino acid sequences were
640 performed using the Clustal W program in MEGA 10.0. The phylogenetic trees were
641 constructed adopting neighbor-joining (NJ) method, using 1000 bootstrap repetitions.

642 All resilin-related and mucin sequences of other model species used in this study are
643 provided as **Figure 4-source data** and **Supplementary file 1**.

644 **Real-time PCR**

645 Total RNA was extracted from thoracic tracheal tubes of each beetle in different
646 treatments using TRIzol reagent according to the manufacturer's protocol and stored at
647 -80°C until used in experiments. The total number of nematodes in corresponding
648 tracheal samples were counted. RNA quality was assessed with an ND-1000
649 spectrophotometer (NanoDrop Technologies, Delaware, USA). About 1 μg of RNA was
650 used as template to produce cDNA with FastQuant RT kit with a genomic DNA eraser
651 (Tiangen, KR106). RT-qPCR was performed using Talent qPCR PreMix (SYBR Green)
652 (Tiangen, FP209) and on a 7300Plus Real-Time PCR system (Applied Biosystems,
653 Massachusetts, USA). At least five biological replicates were assayed for statistical
654 analysis. The amount of mRNA was calculated by the change in cycle threshold (ΔΔCt)
655 method and was normalized to control rp49 mRNA values. qPCR primers are listed in
656 **Supplementary file 2**.

657 **Western blot analysis**

658 Total proteins were extracted from thoracic tracheal tubes of each beetle in different
659 treatments using TRIzol reagent according to the manufacturer's protocol and stored at
660 -80°C until used in experiments. The protein extracts (100 mg) were electrophoresed
661 on 4–12% SDS-PAGE precast gels (EASYBIO, China) and then transferred to 0.22 μm

662 polyvinylidene difluoride (PVDF) membranes (Millipore). The membrane was
663 incubated with polyclonal antibody against target protein (anti-Muc91C, developed by
664 BGI, China, 1:4000). Goat anti-rabbit IgG (EASYBIO, 1:5000) was used as the
665 secondary antibody. Monoclonal antibody against Histone H3 (EASYBIO, 1:2000) was
666 used as an internal control. Goat anti-mouse IgG (EASYBIO, 1:5000) was used as the
667 secondary antibody. Protein bands were detected by SuperSignal West Atto Ultimate
668 Sensitivity Substrate (Invitrogen, A38554).

669 **Whole-mount Immunohistochemistry**

670 Thoracic tracheal tubes of each beetle in different treatments were dissected and
671 instantly fixed with 4% paraformaldehyde overnight. After being washed with 1x PBS
672 buffer, the samples were permeabilized with 0.5% TritonX-100/PBS at 37 ˚C for 20min,
673 then blocked with 5% goat serum for 1 h and incubated with affinity-purified polyclonal
674 rabbit antibody against Muc91C (produced by BGI, China, 1: 100) at 4˚C for 24 h. The
675 samples were then washed 3 times for 5 min each with 0.5% TritonX-100/PBS, Alexa
676 Fluor-488 goat anti-rabbit IgG (Invitrogen, A11008, 1: 500) was used as the secondary
677 antibody. The cellular nucleus was stained with Hoechst 33342 (Invitrogen H3570, 1:
678 1000) for 20 min. The cell membrane system was stained with CellTracker CM-DiI dye
679 (Invitrogen, C7001, 1: 500) for 30 min. Finally, the samples were mounted with
680 Fluoroshield mounting medium (Solarbio, S2100). Fluorescence was detected using an
681 confocal laser-scanning microscope (SP8 Lightning, Leica). Taenidial folds are
682 autofluorescenct excitated by 488nm or 561nm Lasers and have higher

683 autofluorescence excitated by 561nm Laser. Images were processed using LAS X
684 Navigator (Leica).

685 **RNA interference**

686 Double-stranded RNAs (dsRNAs) were synthesized with cDNA templates possessing
687 T7 RNA polymerase promoter sequences on both ends (**Supplementary file 2**),
688 according to the T7 RiboMax Express RNAi System Kit (Promega, P1700) protocol.
689 Within two days after molting, approximately 60 adults beetle were injected at the joint
690 of the second and the third abdominal segment with 30 μg of dsRNA (< 5 μl) using a
691 7000-series modified microliter syringe (Hamilton, Bonaduz, Switzerland). Control
692 beetles were injected with dsGFP as a negative control. The injected adult beetles were
693 kept in standard conditions for four days, then treated with 1% O_2 for 12h. The injected
694 adult beetles used in the nematodes loading trial were kept in 50ml Erlenmeyer flasks
695 with barley medium containing dispersal L_{III} and L_{IV} nematodes at 25°C for 5 days. When
696 the adults were seven days old, they were dissected to obtain trachea samples for the
697 different assays, and disposed as described earlier.

698 **Statistical analysis**

699 The sample size is determined according to previous publications in the pine sawyer
700 beetle species (Wu et al., 2019; Zhao et al., 2016; Zhou et al., 2018). For nematode
701 loading, hypoxic treatments and RNAi treatments, individuals were randomly allocated
702 into experimental group and control group, and no restricted randomization was applied.

703 For nematode quantification, measurements of mechanical properties with tensile
704 testing, researchers were blind to RNAi or hypoxic treatments before counting or
705 measurements. All experiments were performed for at least 3 independent biological
706 replicates.

707 A Pearson correlation coefficient was used to measure the correlation between PWN
708 loading and partial pressure of oxygen. The semi-log fit using least square method was
709 chosen for curve fitting. The fit formula was $Y=10.55 + (-9.629) \times \log(X)$ with an R^2
710 value of 0.85. A Kolmogorov Smirnov test was used to check the normality of data.
711 When the assumption of normal distribution was met, Student's t test and One-way
712 ANOVA with Dunn's or Tukey's multiple comparison were used for two-group and
713 three-group comparisons, respectively. When the assumption of normal distribution
714 was not met, Mann-Whitney U test and Kruskal–Wallis with Dunn's multiple
715 comparison were used for two-group and three-group comparisons, respectively.
716 Statistical analysis was performed with Graphpad Prism 8.0 (Graphpad software, San
717 Diego, California, USA).

718 Acknowledgements

719 This work was funded by the National Natural Science Foundation of China (32088102,
720 32061123002, 32230066 and 31970466) and National Key Research and Development
721 Program of China (2021YFC2600100). We are grateful to Yujia Xiang and Jin Ge for
722 the assistance in bioinformatic analysis. We thank Kathryn E. Bushley for reviewing
723 the manuscript.

Author contribution

X.T., J.Z., L.Z. and J.S. conceived and designed the experiments. J.S. supervised the study. X.T. performed loading and counting of PWN, tracheal dissection, tensile test, Western blot and immunohistochemistry. X.T and J.Z. conducted measurement of oxygen concentrations, TEM and transcriptomic analysis. J.Z. conducted protein purification for polyclonal antibody preparation. X.T. and S.L. performed real-time PCR, RNA interference. S.L. provided the support for visualization of schematic diagram. X.T. prepared the manuscript draft. X.T., J.Z., T. K. and J.S. revised the manuscript.

Additional files

Supplementary files:

Supplementary file 1. Species and GenBank accession no. of Pro-resilins and mucins.

Supplementary file 2. Primers for real-time qPCR and RNAi experiments.

Data availability:

All data generated or analyzed during this study are included in the manuscript and supporting file; Source Data files have been provided for Figures 1, 2, 3, 4, 5 and 6.

The following dataset was generated or analyzed:

Author(s)	Year	Dataset title	Dataset URL	Database and Identifier
Tang X	2022	RNA-seq of pine sawyer beetle with PWN	https://ngdc.cncb.ac.cn/gsa/s/9O83D627	bigd, CRA006464

Tang X	2022	RNA-Seq of tracheal tubes in adult pine sawyer beetle	https://ngdc.cncb.ac.cn/gsa/s/fEsL0f8r	bigd, CRA008617

References

Aikawa T. Transmission Biology of *Bursaphelenchus xylophilus* in Relation to Its Insect Vector[Book Section]. *Pine Wilt Disease*: 2008, 123-138.

Akbulut S, Stamps WT. Insect vectors of the pinewood nematode: a review of the biology and ecology of *Monochamus* species. *Forest Pathology*, 2012, **42**: 89-99. DOI:10.1111/j.1439-0329.2011.00733.x

Andersen SO. Studies on resilin-like gene products in insects. *Insect Biochemistry and Molecular Biology*, 2010, **40**: 541-551. DOI:10.1016/j.ibmb.2010.05.002

Bartholomay LC, Michel K. Mosquito Immunobiology: The Intersection of Vector Health and Vector Competence. *Annual Review of Entomology*, 2018, **63**: 145-167. DOI:10.1146/annurev-ento-010715-023530

Berg JT, Fu Z, Breen EC, Tran H-C, Mathieu-Costello O, West JB. High lung inflation increases mRNA levels of ECM components and growth factors in lung parenchyma. 1997, **83**: 120-128. DOI:10.1152/jappl.1997.83.1.120

Brune A, Emerson D, Breznak JA. The termite gut microflora as an oxygen sink: microelectrode determination of oxygen and pH gradients in guts of lower and higher termites. *Applied And Environmental Microbiology*, 1995, **61**: 2681-2687.

Centanin L, Gorr TA, Wappner P. Tracheal remodelling in response to hypoxia. *Journal of Insect Physiology*, 2010, **56**: 447-454. DOI:10.1016/j.jinsphys.2009.05.008

Chen AYS, Walker GP, Carter D, Ng JCK. A virus capsid component mediates virion retention and transmission by its insect vector. *PNAS*, 2011, **108**: 16777-16782. DOI:10.1073/pnas.1109384108

Chen Y, Chen Q, Li M, Mao Q, Chen H, Wu W, Jia D, Wei T. Autophagy pathway induced by a plant virus facilitates viral spread and transmission by its insect vector. *PLoS Pathogens*, 2017, **13**: e1006727. DOI:10.1371/journal.ppat.1006727

Coon KL, Valzania L, McKinney DA, Vogel KJ, Brown MR, Strand MR. Bacteria-mediated hypoxia functions as a signal for mosquito development. *PNAS*, 2017, **114**: E5362-E5369. DOI:10.1073/pnas.1702983114

Dai J, Estrada B, Jacobs S, Sanchez-Sanchez BJ, Tang J, Ma M, Magadan-Corpas P, Pastor-Pareja JC, Martin-Bermudo MD. Dissection of Nidogen function in *Drosophila* reveals tissue-specific mechanisms of basement membrane assembly. *PLoS Genetics*, 2018, **14**: e1007483. DOI:10.1371/journal.pgen.1007483

Dong B, Hannezo E, Hayashi S. Balance between apical membrane growth and luminal matrix resistance determines epithelial tubule shape. *Cell Reports*, 2014, **7**: 941-950. DOI:10.1016/j.celrep.2014.03.066

Dong B, Hayashi S. Shaping of biological tubes by mechanical interaction of cell and extracellular matrix. *Current Opinion in Genetics & Development*, 2015, **32**: 129-134. DOI:10.1016/j.gde.2015.02.009

Eigenbrode SD, Bosque-Perez NA, Davis TS. Insect-borne plant pathogens and their vectors: ecology, evolution, and complex interactions. *Annual Review of Entomology*, 2018, **63**: 169-191. DOI:10.1146/annurev-ento-020117-043119

Elvin CM, Carr AG, Huson MG, Maxwell JM, Pearson RD, Vuocolo T, Liyou NE, Wong DCC, Merritt DJ, Dixon NE. Synthesis and properties of crosslinked recombinant pro-resilin. *Nature*, 2005, **437**: 999-1002. DOI:10.1038/nature04085

Fielding NJ, Evans HF. The pine wood nematode *Bursaphelenchus xylophilus* (Steiner and Buhrer) Nickle (= *B. lignicolus* Mamiya and Kiyohara): an assessment of the current position. *Forestry*, 1996, **69**: 35-46.

Glasheen BM, Robbins RM, Piette C, Beitel GJ, Page-McCaw A. A matrix metalloproteinase mediates airway remodeling in *Drosophila*. *Developmental Biology*, 2010, **344**: 772-783. DOI:10.1016/j.ydbio.2010.05.504

Graham AM, Barreto FS. Loss of the HIF pathway in a widely distributed intertidal crustacean, the copepod *Tigriopus californicus*. *PNAS*, 2019, **116**: 12913-12918. DOI:10.1073/pnas.1819874116

Gray JS, Estrada-Pena A, Zintl A. Vectors of Babesiosis. *Annual Review of Entomology*, 2019, **64**: 149-165. DOI:10.1146/annurev-ento-011118-111932

Greenlee KJ, Socha JJ, Eubanks HB, Pedersen P, Lee WK, Kirkton SD. Hypoxia-induced compression in the tracheal system of the tobacco hornworm caterpillar, *Manduca sexta*. *Journal of Experimental Biology*, 2013, **216**: 2293-2301. DOI:10.1242/jeb.082479

Hammami A, Abidin BM, Charpentier T, Fabie A, Duguay AP, Heinonen KM, Stager S. HIF-1α is a key regulator in potentiating suppressor activity and limiting the microbicidal capacity of MDSC-like cells during visceral leishmaniasis. *PLoS Pathogens*, 2017, **13**: e1006616. DOI:10.1371/journal.ppat.1006616

Harrison JF, Greenlee KJ, Verberk WCEP. Functional hypoxia in insects: definition, assessment, and consequences for physiology, ecology, and evolution. *Annual Review of Entomology*, 2018, **63**: 303-325. DOI:10.1146/annurev-ento-020117-043145

Hayashi S, Kondo T. Development and function of the *Drosophila* tracheal system. *Genetics*, 2018, **209**: 367-380. DOI:10.1534/genetics.117.300167

Henry JR, Harrison JF. Plastic and evolved responses of larval tracheae and mass to varying atmospheric oxygen content in *Drosophila melanogaster*. *The Journal of Experimental Biology*, 2004, **207**: 3559-3567. DOI:10.1242/jeb.01189

Jang S, Mergaert P, Ohbayashi T, Ishigami K, Shigenobu S, Itoh H, Kikuchi Y. Dual oxidase enables insect gut symbiosis by mediating respiratory network formation. *PNAS*, 2021, **118**: e2020922118. DOI:10.1073/pnas.2020922118

Kaiser NJ, Kant RJ, Minor AJ, Coulombe KLK. Optimizing blended collagen-fibrin hydrogels for cardiac tissue engineering with human iPSC-derived cardiomyocytes. *ACS Biomaterials Science and Engineering*, 2019, **5**: 887-899. DOI:10.1021/acsbiomaterials.8b01112

Kusuma S, Zhao S, Gerecht S. The extracellular matrix is a novel attribute of endothelial progenitors and of hypoxic mature endothelial cells. *FASEB Journal*, 2012, **26**: 4925-4936. DOI:10.1096/fj.12-209296

Lataillade LG, Vazeille M, Obadia T, Madec Y, Mousson L, Kamgang B, Chen CH, Failloux AB, Yen PS. Risk of yellow fever virus transmission in the Asia-Pacific region. *Nature Communications*, 2020, **11**: 5801. DOI:10.1038/s41467-020-19625-9

Lerch S, Zuber R, Gehring N, Wang Y, Eckel B, Klass KD, Lehmann FO, Moussian B. Resilin matrix distribution, variability and function in *Drosophila*. *BMC Biology*, 2020, **18**: 195. DOI:10.1186/s12915-020-00902-4

Litvak Y, Mon KKZ, Nguyen H, Chanthavixay G, Liou M, Velazquez EM, Kutter L, Alcantara MA, Byndloss MX, Tiffany CR, Walker GT, Faber F, Zhu Y, Bronner DN, Byndloss AJ, Tsolis RM, Zhou H, Baumler AJ. Commensal *Enterobacteriaceae* protect against *Salmonella* colonization through oxygen competition. *Cell Host & Microbe*, 2019, **25**: 128-139.e125. DOI:10.1016/j.chom.2018.12.003

Llimargas M, Strigini M, Katidou M, Karagogeos D, Casanova J. Lachesin is a component of a septate junction-based mechanism that controls tube size and epithelial integrity in the *Drosophila* tracheal system. *Development*, 2004, **131**: 181-190. DOI:10.1242/dev.00917

Luschnig S, Bätz T, Armbruster K, Krasnow MA. *Serpentine* and *vermiform* encode matrix proteins with chitin binding and deacetylation domains that limit tracheal tube length in *Drosophila*. *Current Biology*, 2006, **16**: 186-194. DOI:10.1016/j.cub.2005.11.072

Lyons RE, Lesieur E, Kim M, Wong DCC, Huson MG, Nairn KM, Brownlee AG, Pearson RD, Elvin CM. Design and facile production of recombinant resilin-like polypeptides: gene construction and a rapid protein purification method. *Protein Engineering, Design and Selection*, 2007, **20**: 25-32. DOI:10.1093/protein/gzl050

Martens EC, Neumann M, Desai MS. Interactions of commensal and pathogenic microorganisms with the intestinal mucosal barrier. *Nature Reviews Microbiology*, 2018, **16**: 457-470. DOI:10.1038/s41579-018-0036-x

McGettrick AF, Corcoran SE, Barry PJ, McFarland J, Cres C, Curtis AM, Franklin E, Corr SC, Mok KH, Cummins EP, Taylor CT, O'Neill LA, Nolan DP. *Trypanosoma brucei* metabolite indolepyruvate decreases HIF-1alpha and glycolysis in macrophages as a mechanism of innate immune evasion. *PNAS*, 2016, **113**: E7778-E7787. DOI:10.1073/pnas.1608221113

Michels J, Appel E, Gorb SN. Functional diversity of resilin in Arthropoda. *Beilstein Journal of Nanotechnology*, 2016, **7**: 1241-1259. DOI:10.3762/bjnano.7.115

Nairn KM, Lyons RE, Mulder RJ, Mudie ST, Cookson DJ, Lesieur E, Kim M, Lau D, Scholes FH, Elvin CM. A synthetic resilin is largely unstructured. *Biophysical Journal*, 2008, **95**: 3358-3365. DOI:10.1529/biophysj.107.119107

O'Neill K, Olson BJ, Huang N, Unis D, Clem RJ. Rapid selection against arbovirus-induced apoptosis during infection of a mosquito vector. *PNAS*, 2015, **112**: E1152-E1161. DOI:10.1073/pnas.1424469112

Öztürk-Çolak A, Moussian B, Araújo SJ. *Drosophila* chitinous aECM and its cellular interactions during tracheal development. *Developmental Dynamics*, 2016, **245**: 259-267. DOI:10.1002/dvdy

Pettersen EO, Larsen LH, Ramsing NB, Ebbesen P. Pericellular oxygen depletion during ordinary tissue culturing, measured with oxygen microsensors. *Cell Proliferation*, 2005, **38**: 257-267.

Syed ZA, Härd T, Uv A, van Dijk-Härd IF. A potential role for *Drosophila* mucins in development and physiology. *PLOS ONE*, 2008, **3**: e3041. DOI:10.1371/journal.pone.0003041

Tang X, Koski T-M, Sun J. The entry of pinewood nematode is linked to programmed tracheal development of vector beetles. *bioRxiv*, 2022: 2022.2010.2029.514345. DOI:10.1101/2022.10.29.514345

Togashi K, Sekizuka H. Influence of the pine wood nematode, *Bursaphelenchus lignicolus* (Nematoda: Aphelenchoididae), on longevity of its vector, *Monochamus alternatus* (Coleoptera:

Cerambycidae). *Applied Entomology and Zoology*, 1982, **17**: 160-165.

Togashi K. Transmission Curves of *Bursaphelenchus xylophilus* (Nematoda: Aphelenchoididae) from Its Vector, *Monochamus alternatus* (Coleoptera: Cerambycidae), to Pine Trees with Reference to Population Performance. *Applied Entomology and Zoology*, 1985, **20**: 246-251.

Uzest M, Gargani D, Drucker M, Hébrard E, Garzo E, Candresse T, Fereres A, Blanc S. A protein key to plant virus transmission at the tip of the insect vector stylet. *PNAS*, 2007, **104**: 17959-17964.

Valzania L, Coon KL, Vogel KJ, Brown MR, Strand MR. Hypoxia-induced transcription factor signaling is essential for larval growth of the mosquito *Aedes aegypti*. *PNAS*, 2018, **115**: 457-465. DOI:10.1073/pnas.1719063115

Wang S, Guo H, Ge F, Sun Y. Apoptotic neurodegeneration in whitefly promotes the spread of TYLCV. *eLife*, 2020, **9**: e56168. DOI:10.7554/eLife.56168

Webster MR, De Vita R, Twigg JN, Socha JJ. Mechanical properties of tracheal tubes in the American cockroach (*Periplaneta americana*). *Smart Materials and Structures*, 2011, **20**: 094017. DOI:10.1088/0964-1726/20/9/094017

Wei J, He YZ, Guo Q, Guo T, Liu YQ, Zhou XP, Liu SS, Wang XW. Vector development and vitellogenin determine the transovarial transmission of begomoviruses. *PNAS*, 2017, **114**: 6746-6751. DOI:10.1073/pnas.1701720114

Westneat MW, Betz O, Blob RW, Fezzaa K, Cooper WJ, Lee WK. Tracheal respiration in insects visualized with synchrotron x-ray imaging. *Science*, 2003, **299**: 558-560. DOI:doi:10.1126/science.1078008

Wilkin MB, Becker MN, Mulvey D, Phan I, Chao A, Cooper K, Chung HJ, Campbell ID, Baron M, MacIntyre R. *Drosophila* Dumpy is a gigantic extracellular protein required to maintain tension at epidermal–cuticle attachment sites. *Current Biology*, 2000, **10**: 559-567.

Wirtz HR, Dobbs LG. The effects of mechanical forces on lung functions. *Respiration Physiology*, 2000, **119**: 1-17. DOI:10.1016/S0034-5687(99)00092-4

Wu Y, Wickham JD, Zhao L, Sun J. CO_2 drives the pine wood nematode off its insect vector. *Current Biology*, 2019, **29**: R619-R620. DOI:10.1016/j.cub.2019.05.033

Zeitouni NE, Chotikatum S, von Kockritz-Blickwede M, Naim HY. The impact of hypoxia on intestinal epithelial cell functions: consequences for invasion by bacterial pathogens. *Molecular and Cellular Pediatrics*, 2016, **3**: 14. DOI:10.1186/s40348-016-0041-y

Zhao L, Mota M, Vieira P, Butcher RA, Sun J. Interspecific communication between pinewood nematode, its insect vector, and associated microbes. *Trends in Parasitology*, 2014, **30**: 299-308. DOI:10.1016/j.pt.2014.04.007

Zhao L, Zhang X, Wei Y, Zhou J, Zhang W, Qin P, Chinta S, Kong X, Liu Y, Yu H, Hu S, Zou Z, Butcher RA, Sun J. Ascarosides coordinate the dispersal of a plant-parasitic nematode with the metamorphosis of its vector beetle. *Nature Communications*, 2016, **7**: 12341. DOI:10.1038/ncomms12341

Zhao X, Zhang J, Yang J, Niu N, Zhang J, Yang Q. Mucin family genes are essential for the growth and development of the migratory locust, *Locusta migratoria*. *Insect Biochemistry and Molecular Biology*, 2020, **123**: 103404. DOI:10.1016/j.ibmb.2020.103404

Zhou J, Zhao LL, Yu HY, Wang YH, Zhang W, Hu SN, Zou Z, Sun JH. Immune tolerance of vector beetle to its partner plant parasitic nematode modulated by its insect parasitic nematode. *FASEB Journal*, 2018, **32**: 4862-4877. DOI:10.1096/fj.201800247R

Zuo L, Iordanou E, Chandran RR, Jiang L. Novel mechanisms of tube-size regulation revealed by the

Drosophila trachea. *Cell and Tissue Research*, 2013, **354**: 343-354. DOI:10.1007/s00441-013-1673-z

Figure supplements

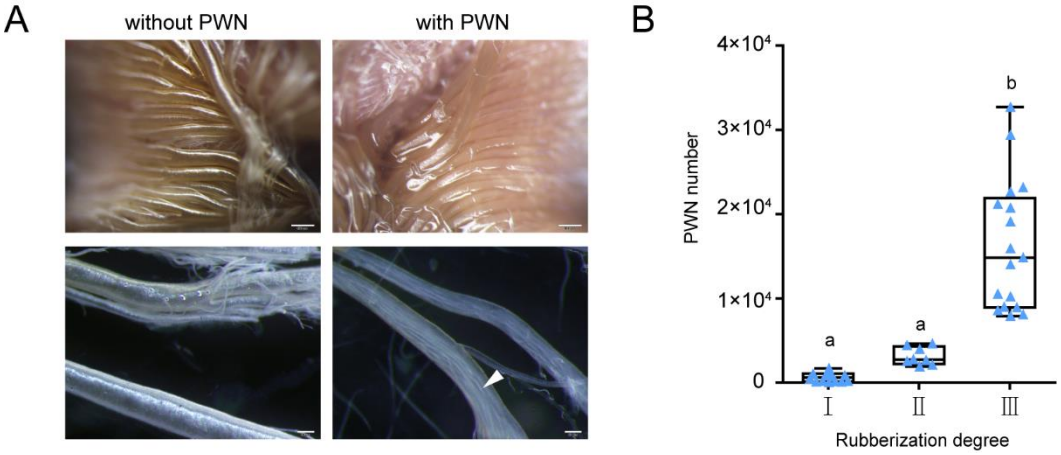

Figure 2-figure supplement 1. Morphological changes of trachea of *M. alternatus* after PWN loading. (**A**) Morphology of thoracic tracheal tubes without and with heavy PWN under stereoscopic microscope. Images in the upper (scale bar = 500μm) or lower (scale bar = 50μm) panel show trachea in vivo and in PBS solution, respectively. White arrow pinpoints PWN inside trachea tubes. Experiments were performed at least three times. (**B**) The relationship between total number of PWN per *M. alternatus* and degree of rubberization. According to the proportion of rubber-like tubes in all thoracic tracheal tubes, we sorted the trachea of beetles with PWN into three rubberization degrees (I, none; II, less than 50% rubber-like tubes; III, 50%~100% rubber-like tubes), and counted the number of PWN released from trachea. 39 adults, $N_I = 14$, $N_{II} = 8$, $N_{III} = 17$. Labels with different letters are significantly different at $P < 0.0001$ (Kruskal-Wallis test, followed by Dunn's multiple comparison test).

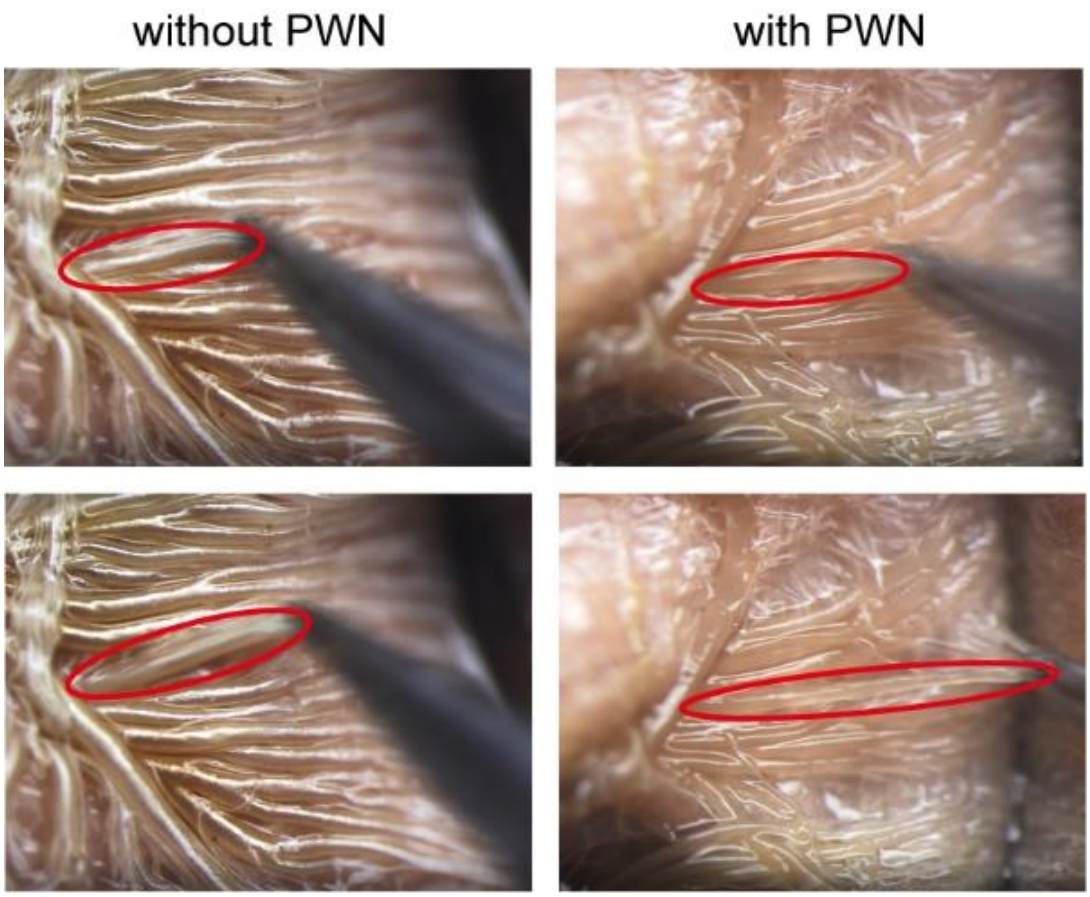

Figure 2-figure supplement 2. Pulling test of trachea of *M. alternatus* after PWN loading. Snapshots from videos imaged under stereotype microscope showed the pulling result of thoracic tracheal tubes with or without PWN. Red circles show one representative tubes in two groups before and after pulling.

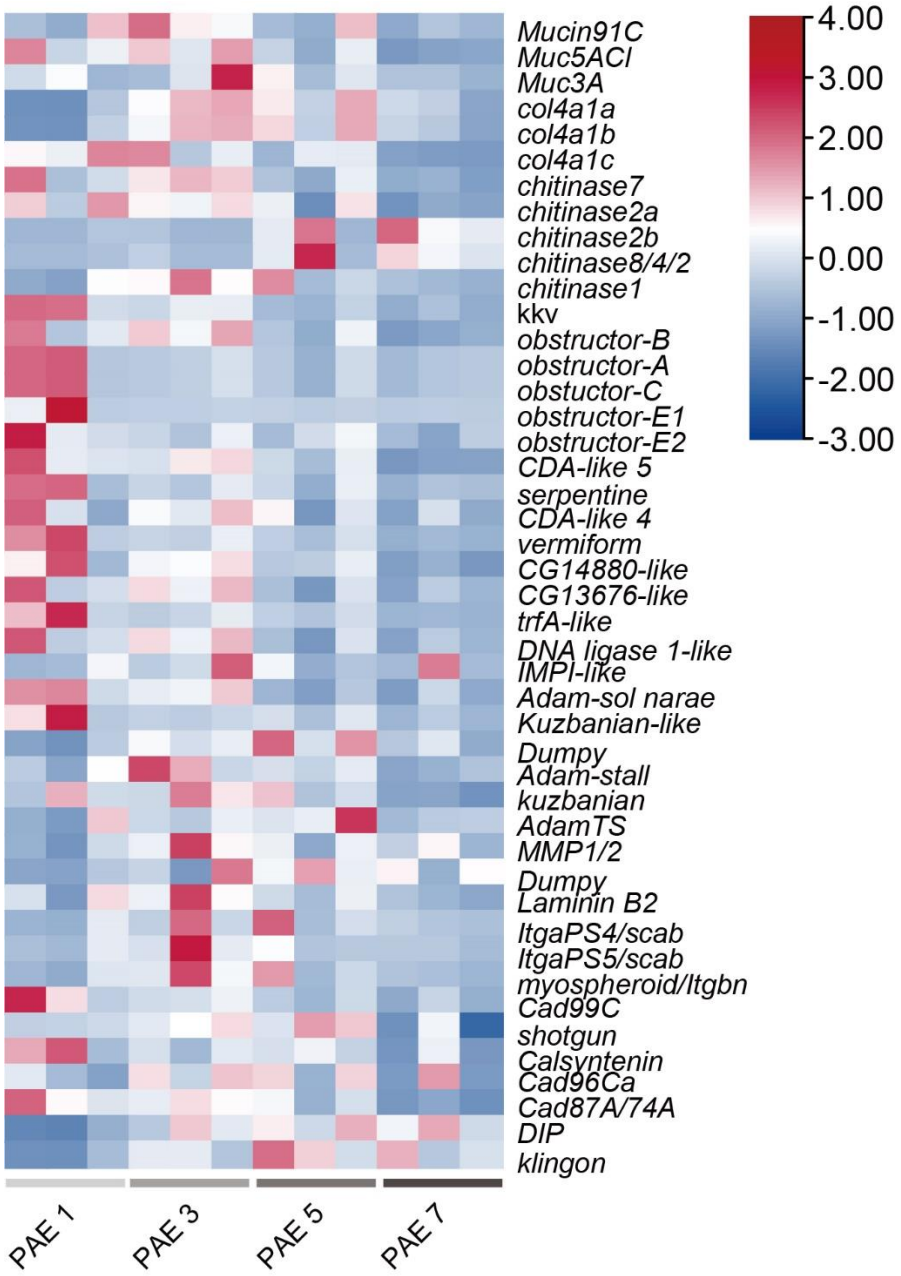

Figure 3-figure supplement 1. Heat map of differential expressed genes related to mechanical property of tracheal tubes of beetles after one day, three days, five days and seven days post eclosion (PAE 1, PAE 3, PAE 5 and PAE 7, respectively)

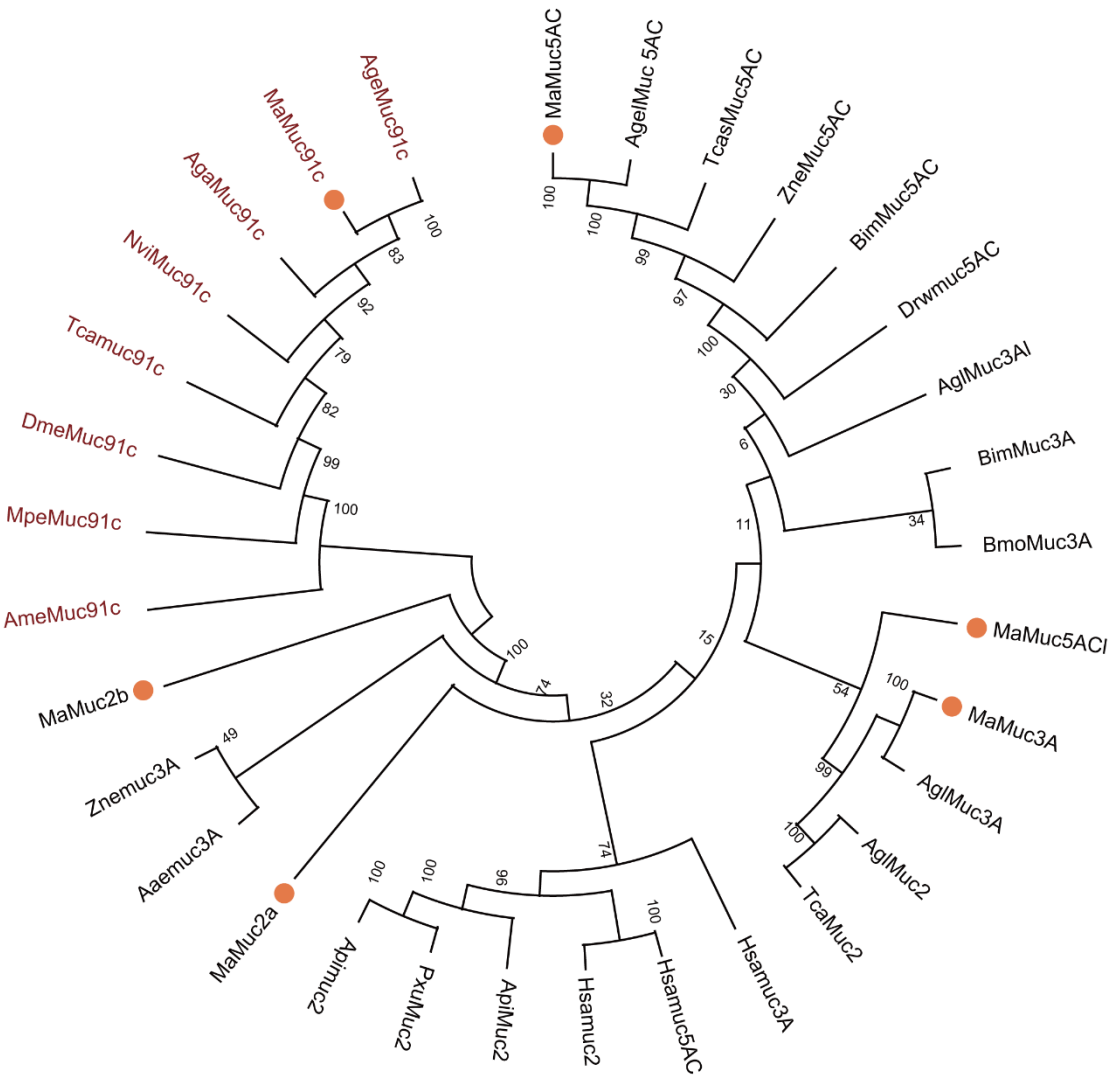

Figure 5-figure supplement 1. A phylogenetic tree constructed using *M. alternatus*. mucin sequences (orange dots) and other species' mucin sequences. Muc91C proteins were highlighted in red font. The full-length amino acid sequences of representative proteins were retrieved from the GenBank database. The phylogenetic tree was constructed with the MEGA 10.0 software based on a multiple alignment of the amino acid sequences performed by Clustal W, and adopting the NJ method. A bootstrap analysis of 1000 replications were used and 50% cut-off bootstrap values were applied to condense the tree. The sequence numbers of mucin or mucin-like proteins are listed in **Supplementary file 1**.

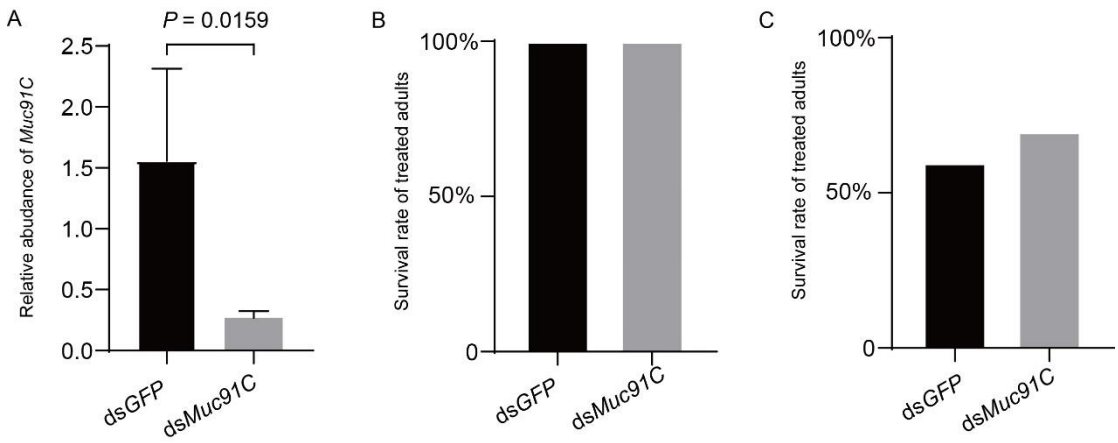

Figure 6-figure supplement 1. RNAi efficiency of the Muc91C gene and survival rates in dsRNA-treated adult beetles. (**A**) Relative abundance of *Muc91C* in *GFP*i and *Muc91C*i beetles. Data are presented as mean ± SEM. $N = 5$. P value is determined by Mann-Whitney U test. (**B**) Accumulated survival rate of adults in RNAi efficiency assessment, TEM imaging and tensile testing. Adults were injected with dsRNA and treated with 1% O_2 for 12h. $N = 20$. (**C**) Survival rate of adults in PWN loading assay. Adults were injected with dsRNA and reared in flasks with barley medium containing PWN. $N = 10$. Difference of proportions was analyzed by Chi-square test.